Characterizing near-surface erosion variability in claypan soils

by

Mark Mathis II

B.S., Kansas State University, 2017

A THESIS

submitted in partial fulfillment of the requirements for the degree

MASTER OF SCIENCE

Department of Civil Engineering
College of Engineering

KANSAS STATE UNIVERSITY
Manhattan, Kansas

2020

Approved by:

Co-Major Professor
Stacey E. Kulesza

Approved by:

Co-Major Professor
Gretchen F. Sassenrath

Copyright

Abstract

Soil erosion due to an underlying claypan layer ultimately impairs water resources and limits crop yield in agricultural fields. Claypan soils cover approximately 40,469 km^2 in the United States and are characterized by a highly impermeable layer underlying surficial soil. The objective of this research was to delineate the variability of soil properties, including soil erodibility, in claypan soils. Understanding how soil properties change in the subsurface is critical to understanding the processes exacerbating soil loss in claypan regions. Geophysical methods were used to determine the spatial variability of surface soil (apparent electrical conductivity) and the soil stratigraphy between a high and low apparent electrical conductivity areas (electrical resistivity tomography). Laboratory (erosion function apparatus) and in-situ ("mini" jet erosion test), erosion methods were used to identify the variability in soil erosion with depth in claypan soils. Laboratory test were used to classify and determine the strength and permeability of claypan soils. The results of this study indicate the surficial soil has a higher hydraulic conductivity and is more erodible than the underling claypan layer, which has a lower hydraulic conductivity and is resistant to erosion. As a result, surficial soil is being eroded by the process of undermining due to an underlying impermeable claypan layer. This research is significant because there is limited knowledge of erosion on claypan soils. The knowledge gained from this study will aid in the quantification of erosion on claypan soils in existing erosion models at field and watershed scales.

Table of Contents

List of Figures

List of Tables

Acknowledgements

First and foremost, I would like to thank my co-advisors, Dr. Stacey Kulesza and Dr. Gretchen Sassenrath, for their continued support and shared knowledge the past two years. They provided me ample opportunities for continued academic growth. The knowledge gained from them will help me throughout the rest of my career. Their high standards for success helped me realize that I was able to accomplish more than I originally imagined. Their passion for their respective fields motivated me to be the best in my career. I am very grateful to have worked with them.

I would also like to thank my officemates, Weston Koehn, Robert Sherwood, Md Zahidul Karim, Luke Augustine, and Saikat Kuili, for their continued support and help performing field and laboratory testing. It was nice to know that whenever I needed assistance, I could rely on them to help me accomplish whatever needed to be completed. I will always consider them friends and it was a joy getting to know them on a personal level. I will cherish the memories created the past two years forever. They were hard working individuals and a joy to work with every day. Without them I don't imagine my graduate school experience would have been the same. I wish them the best of luck in their future endeavors. I extend my thanks to Lonnie Mengarelli and Dekon Strickland for assistance with field work.

Finally, I am grateful to my wife, mom, and dad for always encouraging me and believing in my abilities to do anything I set my mind too. I thank God for the abilities that He blessed me with and for allowing me to accomplish the goals that I set for myself.

Dedication

I would like to dedicate this thesis to my intelligent, generous, and beautiful wife, Cecilia. You gave me my beautiful daughter, Sophia, and I couldn't imagine any success in life without you two in my life. Thank you for supporting and believing in me. Your love and support are the greatest gifts in my life. My success is impossible without you!

Chapter 1 - Introduction

Soil loss is an environmental problem which impacts all aspects of society from impaired water resources to infrastructure stability. Claypan soils are characterized by a highly impermeable layer below surficial soil and covers approximately 40,469 km^2 of the United States (Jamison et al., 1968; Blanco-Canqui et al., 2002). Soil erosion reduces water quality by fostering toxic algal blooms and limiting reservoir capacity by sedimentation (Kansas Water Office, 2016). In agriculture, claypan soils impact crop productivity by restricting root growth, impeding water flow through the subsurface, and limiting soil nutrient availability. Moreover, erosion in claypan soils decreases surficial soil thickness, exposing the impermeable claypan layer at the surface. For example, in Figure 1.1 the creation of an ephemeral gully occurs in an agricultural field due to a shallow surficial soil overlying an impermeable claypan layer in periods of high rainfall. Geophysical, erosion, and laboratory tests were performed in this research to examine the soil properties at two different sites, to better understand the spatial variability in claypan soil erosion.

Figure 1.1. Ephemeral gully erosion.

In this research, geophysical methods included apparent electrical conductivity (EC_a) and electrical resistivity tomography (ERT). Soil EC_a measurements were used to determine the spatial variability of the surface soil. Correlating corn yield measurements and soil EC_a measurements, an area of interest was determined for performing ERT surveys. Therefore, EC_a measurements were used to guide the location of ERT surveys. ERT surveys were performed moving from an area where a suspected claypan layer was near the surface (i.e., high EC_a area) to an area where there was no suspected underlying claypan layer (i.e., low EC_a area). Unlike EC_a measurements, ERT measurements allowed for the determination of changing soil stratigraphy between a high EC_a area and low EC_a area with depth. ERT measurements at both sites guided the location of disturbed and undisturbed soil sample collection. Two different erosion methods (i.e., erosion function apparatus (EFA) and "mini" jet erosion test (JET)) were used to identify the variability in soil erosion with depth in claypan soils. The EFA is a laboratory test that directly measured the erosion rate of undisturbed soil samples due to sheet flow erosion at high hydraulic loading; whereas the JET is an in situ test which directly measured the erosion rate due to free-fall erosion without sample disturbance. The goal of the erosion testing was to obtain the critical shear stress. The critical shear stress is the applied hydraulic stress at which a soil starts to erode (Bernhardt et al., 2011) and a higher critical shear stress indicates that a soil is more erosion-resistant. This research combined surface EC_a measurements, ERT surveys, EFA tests, and JET to characterize where soil erosion was likely occurring. Laboratory tests included soil classification, undrained shear strength, and hydraulic conductivity testing of samples collected in a high and low EC_a area. Soil undrained shear strength may aid in determining erosion potential between distinct soil layers. The hydraulic conductivity may aid in understanding the interaction of water flow between two distinct soil layers. The goal of laboratory tests was to characterize the soil properties of claypan soils to better understand the process by which surficial soil was being eroded.

The objective of this research was to delineate the variability of soil properties, including soil erodibility, in claypan soils. Understanding how soil properties change with the soil profile is critical to understanding the processes exacerbating soil loss in claypan regions. This research is significant because there is limited knowledge on the processes driving surficial soil erosion in claypan regions. The knowledge gained on erosion processes in claypan regions will contribute data for modeling, allowing more accurate simulation of soil losses at field and watershed scales.

There are six chapters in this thesis. The problem statement, background, and the research objective are described in Chapter 1 - . In Chapter 2 - , a detailed literature review on claypan soils, soil erosion, erosion devices, and geophysical tests used in this research are described. The methodology of this research including the site description, EC_a test, setup for ERT surveys, subsurface sampling, test procedure for the EFA test and JET, and procedures for laboratory tests are provided in Chapter 3 - . Chapter 4 - presents the results for both sites. Next, **Error! Reference source not found.** is the discussion of the results. Finally, the conclusions and recommendations for future work are provided in Chapter 6 - .

Chapter 2 - Literature Review

2.1 Claypan soils

Claypan soil formation and characteristics

Claypan soils cover approximately four million hectares in the central United States, including portions of southern Illinois, northeastern and southwestern Missouri, southeastern Kansas and Oklahoma, and northwestern Texas (USDA-NRCS, 2006). Claypan soils are characterized by a dense, compact, and slowly permeable subsurface layer that contains higher clay-sized particle percentage than overlying materials, from which it is separated by a sharp boundary (Soil Science Terms committee, 2008). There is no clear delineation of clay-sized particle percentage, but a typical description is a sharp increase in clay-sized particles over an abrupt boundary (Buckley et al., 2008). The major mechanism in claypan soil formation is a change in parent material stratigraphy. In southeastern Kansas, the claypan soils are formed by clay translocation and loess deposition on top of clayey alluvium or residuum weathered mainly from Permian and Pennsylvanian sandstone, shale, and limestone (Hartley et al., 2014). The formation of claypan soil directly influences its physical, geochemical, and biological properties (Fanning and Gray, 1959; Schaetzl and Thompson, 2015).

2.2 Soil erosion

Erosion rate and critical shear stress

Erosion is the process of soil loss due to water flow and occurs when erosive forces exceed the resistive forces (i.e., gravity, cohesion, and adhesion) within the soil (Winterwerp and van Kesteren, 2004; Sanford, 2008; Grabowski et al., 2011). Erodibility is a measure of these resistive forces and is often expressed as a threshold for erosion (Sanford, 2008; Grabowski et al., 2011). Erosion rate, $\boldsymbol{\varepsilon_r}$, is the mass of sediment eroded per unit time once the erosion threshold exceeds the critical shear stress of the soil. Critical shear stress, $\boldsymbol{\tau_c}$, is the shear stress exerted by flowing water on the soil surface that initiates erosion. A shear stress lower than the critical shear stress will not cause the soil to erode. So, a soil resistant to erosion will have low erodibility and a high critical shear stress; conversely, a highly erodible soil will have high erodibility and a low critical shear stress. The excess shear stress equation is commonly used to describe cohesive soil erosion (Partheniades, 1965; Hanson, 1990a, 1990b; Al-Madhhachi et al., 2013). The excess shear stress equation is:

$$\varepsilon_r = k_d(\tau - \tau_c)^a \qquad \textbf{Equation 2.1}$$

where ε_r is the erosion rate (m s^{-1}), k_d is the rate of soil erosion when the boundary shear stress is greater than the critical shear stress (m^3 (N-s)$^{-1}$), τ is the shear stress exerted on the soil surface (Pa), and τ_c is the critical shear stress (Pa). The empirical exponent a is usually assumed to be unity (Hanson and Cook, 1997; Al-Madhhachi et al., 2013) although researchers have determined a can be as high as 6.8 (Van Klaveren and McCool, 1998; Knapen et al., 2007). Research conducted by Smerdon and Beasley (1959), Kamphius and Hall (1983), Hanson (1996), and Briaud et al. (2001) have tried to find a simple relationship between k_d or τ_c to other soil index parameters (i.e., plasticity index or percent clay) of cohesive soils. However, Grabowski et al. (2011) suggested that erosion of cohesive soils is a complex system dependent on different physical, chemical, and biological factors as shown in Figure 2.1.

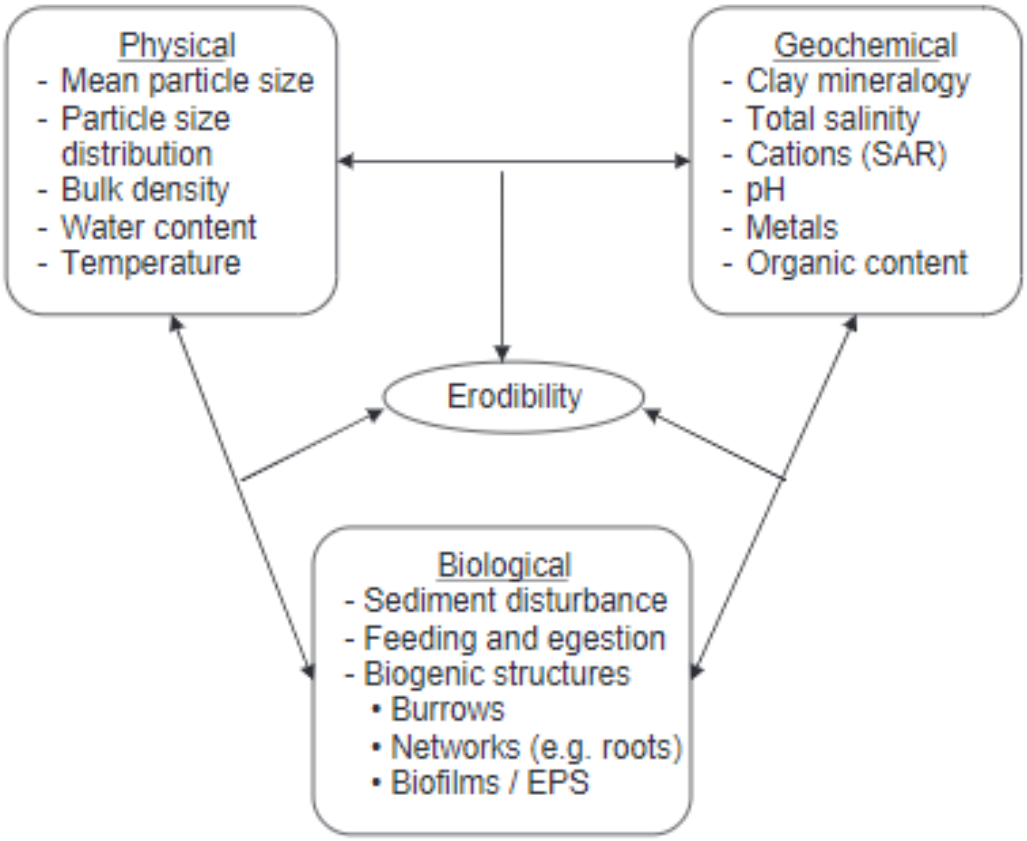

Figure 2.1. Factors affecting erosion in cohesive soils. (Grabowski et al., 2011)

Factor affecting erodibility

Dry unit weight. Hanson and Robinson (1993) conducted a study on compacted clay samples to determine a relationship between the jet index (J_i) and dry unit weight. The jet index is a dimensionless parameter that characterizes erosion potential. The relationship between the jet index and dry unit weight is shown in Figure 2.2. The results showed as dry unit weight increased the jet index decreased. Hanson (1991) developed a relation between the jet index (J_i) and the max depth of scour measurements (D_s) from the submerged jet erosion test. The relationship between the jet index and the maximum depth of scour measurements is:

$$\frac{D_s}{t} = J_i U_o \left(\frac{t}{t_1}\right)^{-0.931} \qquad \textbf{Equation 2.2}$$

where D_s is the maximum depth of scour (cm), t is the time (s), J_i is the jet index (unitless), U_0 is the jet nozzle velocity (cm s^{-1}), and t_1 is the time equivalent of 1 s if t is in time units other than seconds A jet index value of 0.02 indicated a high erodibility, whereas a value of 0.002 indicated a low erodibility. Therefore, clay soil was more erodible at a relatively high jet index (0.02) and low dry unit weight, whereas the clay soil was more erosion-resistant at a higher dry unit weight and low jet index (0.002).

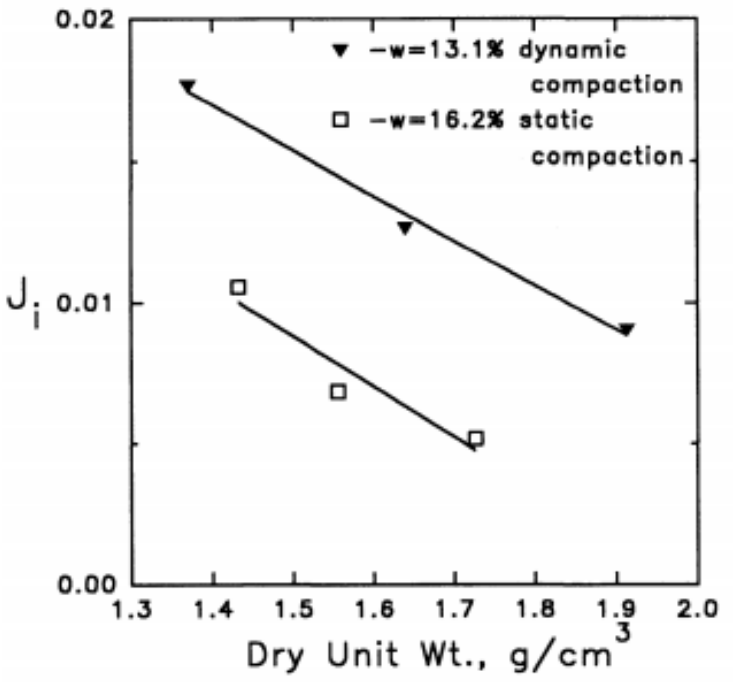

Figure 2.2. Relationship between erosion potential and dry unit weight. (Hanson and Robinson, 1993)

Water content. Hanson and Robinson (1993) also correlated the jet index and water content from four dynamically compacted and three statically compacted clay samples (Figure 2.3). Dynamic compaction was accomplished by dropping a 79.4-kg hammer 30 cm and controlling the number of blows. Static load compaction was achieved by using a pneumatic press to apply loads of up to 46 kN. The clay soil parameters exhibited a liquid limit of 23, a plasticity index between 7 and 12, a maximum dry unit weight of 1.92 g cm^{-3}, an optimum water content of 12.5%, and was classified as a CL or CL-ML according to the Unified Soil Classification System. The compacted dry unit weight was determined by dividing the weight of the solid in the soil element by the total volume occupied by the entire element. The compacted dry unit weight remained constant throughout the seven compacted clay samples. The results showed that the erosion resistance of the soil material is sensitive to water content at the time of compaction. Also, the erosion resistance increased as the water content increased. It was noted that the resistance decreased for the sample compacted at saturation which suggested that there may be an optimum water content slightly less than saturation. As previously noted, a jet index of 0.02 indicated a high erodibility (low resistance to erosion), whereas a value of 0.002 would indicate a low erodibility (high resistance to erosion).

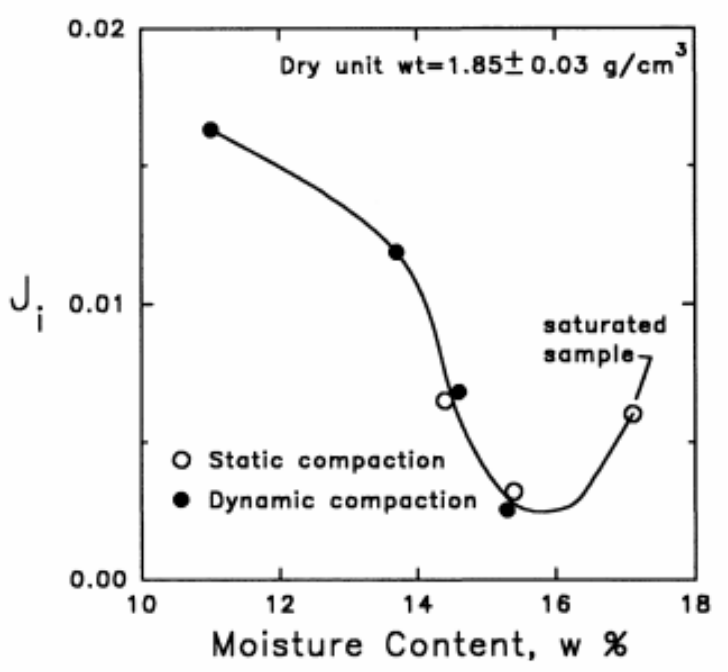

Figure 2.3. Relationship between erosion potential and water content. (Hanson and Robinson, 1993)

Soil compaction. The magnitude of compaction of fine-grained soils strongly influences soil behavior (Lambe and Whiteman, 1979). Laflen and Beasley (1960), Enger (1963), Lyle and Smerdon (1965), Grissinger (1966), Kuti and Yen (1976), Shaikh et al. (1988), and Hanson (1992) have examined the relationship between soil compaction and erosion potential. Hanson and Robinson (1993) evaluated the relationship between the jet index (i.e., erosion potential) of clay samples and compaction technique (i.e., dynamic or static). Three clay samples were dynamically compacted at a gravimetric water content of 13.1% and three clay samples were statically compacted at a gravimetric water content of 16.2%. The jet index of these samples were measured with a submerged jet apparatus. The results, previously shown in Figure 2.2, showed the dynamically and statically compacted clay samples had the same general trend. Hanson and Robinson (1993) also noted that soils compacted at similar unit weights and water contents showed insignificant difference in erosion which indicated that water content and dry unit weight were the dominant variables controlling erosion potential of compacted soils.

Types of erosion

Soil erosion is a complex phenomenon investigated across many disciplines. Soil erosion by water flow is generally divided into three categories: sheet, rill, and gully (Hillel, 2004). Sheet erosion is the removal of thin layers of soil from a more or less smooth slope, carried by the distributed (rather than concentrated) flow of runoff water over the soil surface. Watson and Laflen (1986) described sheet flow erosion as inter-rill erosion and developed an empirical equation to determine the inter-rill erosion rate. The inter-rill erosion rate can be calculated as:

$$D_i = K_i i^2 S_f \qquad \textbf{Equation 2.3}$$

where D_i is the inter-rill erosion rate (kg m^{-2} s^{-1}), K_i is the inter-rill soil erodibility (kg s m^{-4}), i is the rainfall intensity (m s^{-1}), and S_f is an empirical slope factor (unitless). As sheet erosion continues and is repeated over the course of successive rainstorms rill erosion occurs (Hillel, 2004). Rill erosion is the scouring and transport of soil by a concentrated flow of water (Schwab et al., 1993; Hillel, 2004). An empirical equation to calculate the rill detachment rate can be determined as:

$$D_r = K_r(\tau_r - \tau_c)\left(1 - \frac{Q_s}{T_c}\right) \qquad \textbf{Equation 2.4}$$

where D_r is the rill detachment rate (kg m^{-2} s^{-1}), K_r is the rill erodibility (s m^{-1}), τ_r is the hydraulic shear stress of the water flowing in the rill (Pa), τ_c is the critical shear stress of the soil (Pa), Q_s is

the rate of sediment flow in the rill (kg m^{-1} s^{-1}), and T_c is the sediment transport capacity of the rill (kg m^{-1} s^{-1}). As rill erosion continues the rill gradually becomes deeper and forms a gully. The formation of gullies occurs from the process of continued scour into the soil subsurface until eventually reaching a practically impervious subsoil. Soil erosion may decrease at the bottom of the gully but further erosion may occur along the slumping sides of the gullies (Hillel, 2004).

2.3 Erosion devices

Erosion function apparatus (EFA)

The EFA was originally developed to measure the erosion rate of fine-grained soils for bridge scour. In an EFA test, a thinned walled Shelby tube containing a soil sample is placed flushed into an opening in the 1.33 m long rectangular flume with the cross-section of 101.6 x 50.8 m. A pump is used to drive the flow of water over the soil sample in the flume. As the soil erodes, a piston is pushed upwards to extrude the sample from the Shelby tube such that the top of the sample is always kept flush with the flume bottom during testing. The amount of sample eroded is equal to the length of sample lifted by the piston during each velocity, the movement of the piston is automatically measured in the EFA. The temperature of the water in the flume is maintained constant throughout testing as increased water temperature also increases soil erodibility (Tran et al., 2019). The sample is tested for one hour at water velocities of 1, 2, 3, 4, 5, and 6 m/s. After each velocity test, two photographs of the soil surface are taken and processed with a custom photogrammetry computational program to compute the soil surface roughness (as described by Tran et al., 2017). The applied hydraulic shear stress on the surface of the sample, $\boldsymbol{\tau}$ (Pa), and erosion rate, $\dot{\boldsymbol{z}}$ (mm/hr), is calculated for each velocity. The equations for calculating the applied hydraulic shear stress and erosion rate at each velocity are described in Chapter 3 - . These data are used to create a plot of erosion rate versus shear stress for each sample on a hydraulic engineering circular no. 18 (HEC-18) graph to characterize the erosion potential of the soil.

"Mini" jet erosion test (JET)

The "original" JET apparatus was developed by the United States Department of Agriculture - Agricultural Research Service (Hanson, 1990b) for testing the in situ erodibility of surface materials. The JET apparatus has been used for the assessment of the erosion of cohesive soils in river channel degradation, bridge scour, and earthen spillway erosion. Hanson (1991) developed a soil-dependent jet index to empirically relate resistance of a soil to erosion. However, Hanson et

al. (2002) later developed an analytical procedure based on the jet diffusion principles (Stein et al., 1993) to remove empiricism for determining soil erodibility. The Hanson et al. (2002) analytical procedures for determining soil erodibility parameters for a submerged circular jet followed the basis of the jet diffusion principles developed for a submerged planar jet impinging on a soil surface developed by Stein et al. (1993). The "mini" JET apparatus is a modified version of the "original" JET apparatus and was developed to increase the convenience and flexibility of in situ and laboratory testing.

The "mini" JET apparatus (JET here after) can be used for any type of soil but the time interval for which scour is measured throughout jet-testing will vary between cohesionless and cohesive soils. Suggested scour measurements for cohesionless soil is every one to five minutes and every five to ten minutes for cohesive soil (Al-Madhhachi et al., 2011). Scour of the soil surface beneath the hydraulic jet is measured over two hours and at least 10 to 12 scour measurements are recommended for analysis purposes. The procedure for the JET setup followed Hanson and Cook (2004). The Blaisdell method and scour depth method were used for predicting the critical shear stress of the soil in this research. The Blaisdell method predicts the critical shear stress based on estimates of equilibrium scour at time equal to infinity. An alternate method, the scour depth method, uses an iterative approach that minimizes the error between measured and estimated scour depths in solving for the critical shear stress (Wahl, 2016). The Blaisdell method tends to under-predict the critical shear stress, caused by its tendency to yield large estimates of the equilibrium scour depth (Karamigolbaghi et al., 2017). Conversely, the scour depth method tends to over-predict the critical shear stress. The scour depth method was used to determine the critical shear stress from JET data in this research because the estimated scour depth measurements closely followed the observed scour measurements in all JET measurements. The equations for calculating the critical shear stress are described in Chapter 3 - .

2.4 Geophysical tests

Apparent electrical conductivity (EC_a)

Soil electrical conductivity is a measure of the ability of a material to transmit (i.e., conduct) an electrical current through a representative volume of soil. Soil EC_a is a bulk measurement and is affected by different soil properties, including soil clay content, soil water content, bulk density, temperature, and salinity (Rhoades et al., 1989). Soil EC_a is a function of soil particle size and

texture; as such, it is useful in identifying the soil type. As shown in Figure 2.4, sands have a low conductivity, silts have medium conductivity, and clays have high conductivity.

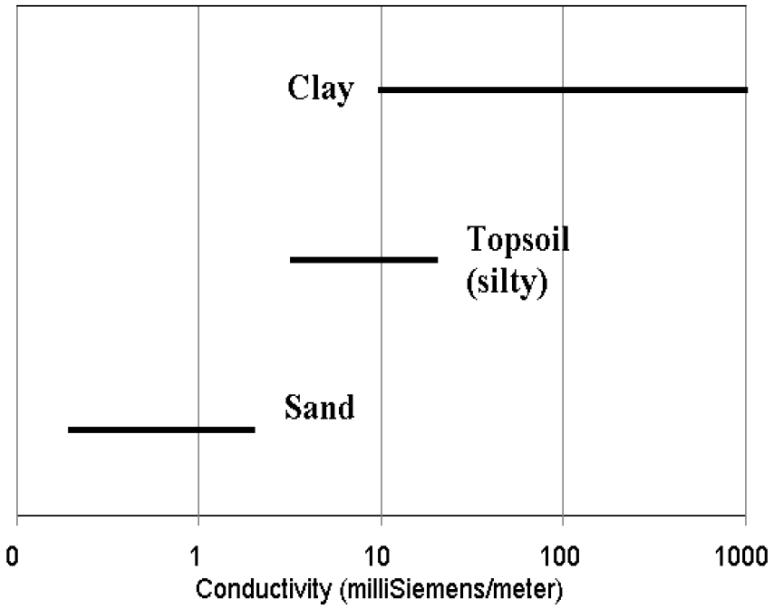

Figure 2.4. Soil type conductivity variation. (Lund and Christy, 1998)

The standard units of measure of EC_a are milliSiemens per meter (mS m^{-1}). Siemens are the inverse of Ohms and are the measurement of a material's conductance (Lund and Christy, 1998). Therefore, one mS m^{-1} is equivalent to 1000 Ohm-m. Ohm-m are the common units for electrical resistivity described in the next section. The software used in this study reports EC_a units in μS cm^{-1}. A Veris model 3100 sensor cart system (Veris Technologies of Salina, KS), in concert with a global positioning system mounted on a tractor, was used to create a soil EC_a map which quantitatively delineated similar and contrasting regions of a field. The system used six 43 cm diameter disc electrodes that remain in direct contact with the soil at a depth of approximately 6 cm. The Veris system uses two discs that serve as the current/sink and the remaining two-disc electrodes measure the resulting voltage potential at the surface. The disc spacing controls the depth of penetration of the electrical survey, which were 30 cm and 80 cm vertical depth in the soil profile in this study. The main advantage of soil EC_a measurements is the ability to quickly collect data over large areas as opposed to discrete sampling methods. The disadvantage of soil EC_a measurements is that data are only collected near-surface (30 cm - 80 cm). The measurement of EC_a is a valuable tool used for identifying the soil physical-chemical properties influencing crop yield patterns and for establishing the spatial variation of soil properties (Corwin et al., 2003b).

Studies conducted in Missouri (Kitchen et al., 1996) and central Iowa (Jaynes et al., 1995) showed substantial correlation between soil EC_a and crop yield. EC_a of clay soil has also been used to predict the depth of surface soil overlying a clay layer (e.g., Doolittle et al., 1994; Jaynes, 1996; Kitchens et al., 2003). Data processing is not needed for this test due to the shallow depth of measurement. It is assumed that the representative volume of soil in each EC_a measurement is homogenous within the spatial resolution of surface EC_a mapper (Friedman, 2005).

Electrical resistivity tomography (ERT)

Electrical resistivity tomography is a near-surface geophysical method commonly used to delineate soil stratigraphy (Groves et al., 2011). The term "near-surface" generally means down to approximately 9 m in the subsurface. ERT has been used for identifying bridge foundations (Arjweh et al., 2013), mapping landfills (Bernstone et al., 2000), predicting soil erodibility (Karim and Tucker-Kulesza, 2018), and geotechnical site characterization (Hiltunen and Roth, 2003). Electrical resistivity is the reciprocal measurement of electrical conductivity; therefore, both systems measure differences in the same soil properties. ERT measurements are different than surface electrical conductivity measurements because ERT collects a "slice" of data into the subsurface, as opposed to only spatial variability at the surface. Relative measurements, like those collected in an electrical conductivity survey, are collected; however, in ERT surveys the data are mathematically inverted to yield the true electrical resistivity of the changing soil properties with depth.

In a four-electrode ERT survey, an electrical current (*I*) is injected into the ground through a current/sink electrode pair (A,B) and the resulting voltage potential (*V*) is measured across another electrode pair (P,Q) a depth below the surface as shown in Figure 2.5.

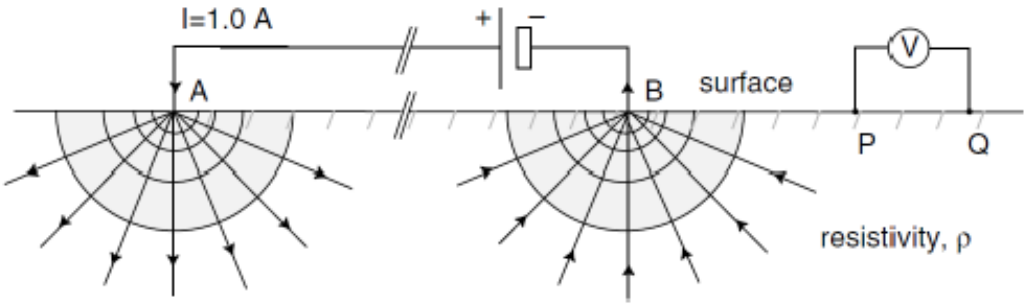

Figure 2.5. Schematic of the source/sink electrode pair (A,B) and voltage potential electrode pair (P,Q). (Everett, 2013)

In Figure 2.5, the voltage potential measured between electrodes P and Q, V_{PQ}, from the current/sink electrode pair (A,B) is calculated as:

$$V_{PQ} = V_P - V_Q = \left(\frac{I\rho}{2\pi}\right)\left[\frac{1}{r_{AP}} - \frac{1}{r_{AQ}} - \frac{1}{r_{BP}} + \frac{1}{r_{BQ}}\right]^{-1} \quad \textbf{Equation 2.5}$$

where ρ is the resistivity in the subsurface (Ohm-m), r_{AP} is the distance between current electrode A and voltage electrode P, r_{AQ} is the distance between current electrode A and voltage electrode Q, r_{BP}. is the distance between sink electrode B and voltage electrode P, and r_{BQ} is the distance between sink electrode B and voltage electrode Q. Note that current flows radially outward creating a hemispherical electric field in the subsurface because current cannot flow through the non-conducting air. In the field, V_{PQ} and I are measured. Rearranging equation 2.5, the resistivity in the subsurface, ρ, is obtained. The resistivity in the subsurface is assumed to be homogenous with uniform resistivity; therefore, the resistivity is called apparent resistivity, ρ_a (Ohm-m). The apparent resistivity is calculated as:

$$\rho_a = \frac{V_{PQ}}{I} * k \quad \textbf{Equation 2.6}$$

where $k = 2\pi\left[\frac{1}{r_{AP}} - \frac{1}{r_{AQ}} - \frac{1}{r_{BP}} + \frac{1}{r_{BQ}}\right]^{-1}$ is the geometric factor for a four-electrode ERT survey

In this research, a 56-electrode ERT survey was performed utilizing a hybrid array (arrays are discussed below). This hybrid inverted Schlumberger and Dipole-dipole array produced high lateral and high vertical resolution.

Multi-channel array types

The advancement of data acquisition systems allows for the collection of multiple electrical resistivity measurements with a single current injection. The current/sink electrode pair (A,B) and potential electrode pair (P,Q) configuration is different in each array. Depth of penetration, signal-to-noise ratio, lateral and vertical resolution are criteria used to determine which array type will yield optimum results for a particular study (Everett, 2013). A hybrid array is a combination of two or more array types and allows for higher resolution of the subsurface composition. In this research, a hybrid array, which included the Dipole-dipole and inverted Schlumberger arrays, is selected because high lateral and vertical resolution is needed to accurately image the soil stratigraphy of near-surface soils. A Wenner array is used in the Veris 3100 system to collect electrical conductivity measurements at the surface. Each array type is described below.

Schlumberger array. Schlumberger array is designed for determining the Earth resistivity profile beneath a single location, also called sounding (Everett, 2013). In Figure 2.6, using a four-electrode ERT survey, the potential electrode pair (P,Q) are kept centered at a fixed location with constant separation 2*a*. The current/sink electrode pair (A,B) are centered at the same location but voltage readings are made as the separation between them is expanded about the common midpoint. Apparent resistivity, ρ_a, is expressed as a function of half the spacing between the current/sink electrodes. Excellent depth penetration is achieved with a large current/sink-potential electrode separation and high vertical resolution is typical of this array. In this research, a hybrid array which included an inverted Schlumberger array was selected because it allows for the collection of multiple resistivity measurements from a single current injection. An inverted Schlumberger array is opposite the Schlumberger array in that the current/sink electrode pair (A,B) is centered at a fixed location inside the potential electrode pair (P,Q). In this way, the voltage readings are made as the separation between the potential electrode pair is expanded about the current/sink electrode pair.

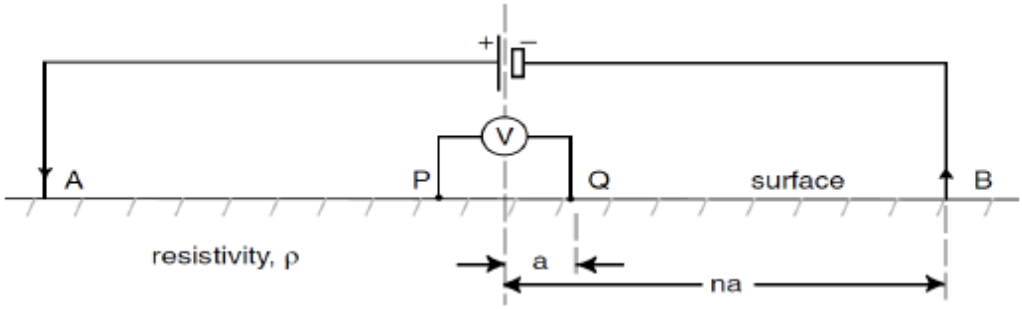

Figure 2.6. Four-electrode Schlumberger array configuration. (Everett, 2013)

Dipole-dipole array. Dipole-dipole array offers advantages of both Schlumberger depth sounding and Wenner lateral profiling (Everett, 2013). For this reason, this array is one of the most popular arrays in resistivity applications (Loke, 1999). In Figure 2.7, using a four-electrode ERT survey, the current/sink electrode pair (A,B) and potential electrode pair (P,Q) have the same spacing *a* but the two pairs are separated by a distance *na*. A disadvantage of this array is the distortion of voltage measurements across the potential electrode pair by small-scale, near-surface heterogeneities caused by the deterioration of the signal-to-noise ratio at large values of *n*.

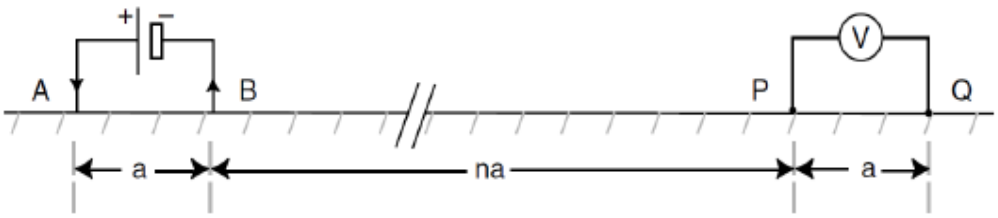

Figure 2.7. Four-electrode Dipole-dipole array configuration. (Everett, 2013)

Wenner array. Wenner array is designed for lateral profiling of the Earth resistivity at a roughly constant depth of penetration (Everett, 2013). The current/sink electrode pair (A,B) and potential electrode pair (P,Q) follow a similar four-electrode configuration as the Schlumberger array where the potential electrode pair (P,Q) is placed inside the current/sink electrode pair (A,B). Unlike the Schlumberger array, the Wenner array has a fixed separation of *a* between the current/sink electrode pair and potential electrode pair as shown in Figure 2.8. In this array, the depth of penetration into the subsurface depends on the *a* spacing. Hence, the larger the *a* spacing the greater depth of penetration and vice versa.

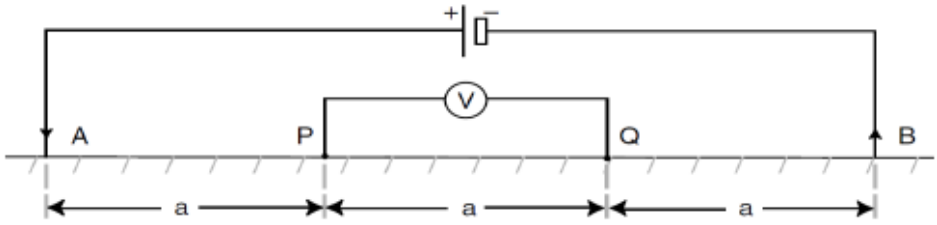

Figure 2.8. Four-electrode Wenner array configuration. (Everett, 2013)

Data processing: forward modeling and data inversion

The purpose for performing a multi-electrode ERT survey is to estimate the apparent resistivity of the subsurface. The pseudosection contouring method is typically used to plot the apparent resistivity ($(\rho_a)_i$) measurements from a 2-D imaging survey (Loke, 1999), as shown in Figure 2.9.

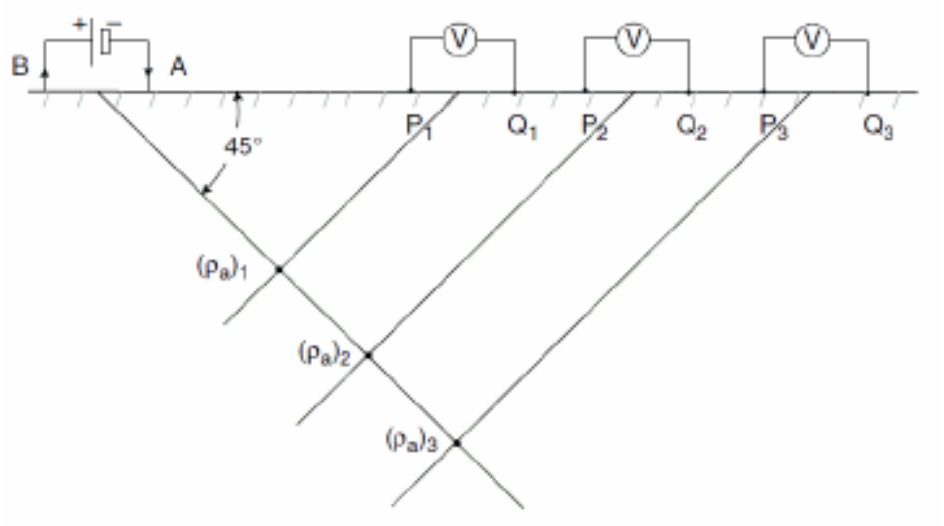

Figure 2.9. Resistivity pseudosection for a Dipole-dipole array. (Everett, 2013)

The apparent resistivity measurements were plotted such that an electrical current is shown at the center of the current/sink electrode pair (A,B) and the voltage potential is shown at the center of the corresponding potential electrode pair (P,Q). Note that the current/sink electrode pair and potential electrode is plotted at the intersection of the 45-degree angle from the horizontal drawn from the center of the electrodes (Hallof, 1957). The corresponding apparent resistivity is measured at a depth below the surface where the current/sink electrode pair and the corresponding potential electrode pair intersect each other. This procedure is repeated until all the current/sink electrode pairs and potential electrode pairs are covered. An estimate of the true subsurface resistivity is obtained (Everett, 2013); however, the pseudosection gives a distorted picture of the subsurface so the measured apparent resistivity is inverted through an iterative process to produce a true representation of the subsurface.

In this research, EarthImager 2D software was used to model and invert the measured apparent resistivity to obtain a subsurface resistivity distribution which was closely correlated with the true subsurface geology. Forward modeling mathematically models the apparent resistivity for given electrical properties and boundary condition using Fourier-transformed partial differential equations (Binley et al., 2005); similarly, data inversion produces the subsurface distribution of electrical properties from a set of given measurements. A 2.5D resistivity forward model using numerical methods by discretization of the domain investigation is used because earth is modeled as 2D but an electrical field due to a point source is modeled as 3D. Therefore, to reduce computing time, the governing 3D partial differential equation is Fourier-transformed into a 2D equation

(AGI, 2007). The forward solution is obtained by solving the 2D partial differential equation in the Fourier transform domain as:

$$\frac{\partial}{\partial x}\left(\sigma\frac{\partial V}{\partial x}\right) + \frac{\partial}{\partial z}\left(\sigma\frac{\partial V}{\partial z}\right) - k^2\sigma V = -I * \delta(x) * \delta(z) \qquad \textbf{Equation 2.7}$$

where V is the scalar electrical potential in the Fourier transform domain, I is the electrical current source, k is the wavenumber in the transform domain, and σ is the electrical conductivity as a function of (x,z). The procedure for resistivity measurement inversion begins by constructing a resistivity model based on the subsurface average apparent resistivity distribution. Next, forward modeling is performed to predict (or, calculate) the apparent resistivity distribution. Then the root mean squared error is used to characterize the goodness of fit between field apparent resistivity measurements and calculated resistivity measurements of the reconstructed model. Note that RMS error gives an average data misfit over all data points. The RMS error (%) is calculated as:

$$RMS = \sqrt{\frac{\sum_{i=1}^{N}\left(\frac{d_i^{Pred} - d_i^{Meas}}{d_i^{Meas}}\right)^2}{N}} \times 100\% \qquad \textbf{Equation 2.8}$$

where N is the total number of measurements, d^{Pred} is the predicted data, and d^{Meas} is the measured data. Another measure of data misfit is the normalized L2-norm. Unlike RMS error, the L2-norm is defined as the sum of the squared weighted data error. The L2-norm is calculated as:

$$L2 - Norm = \sum_{i=1}^{N}\left(\frac{d_i^{Calc} - d_i^{Meas}}{W_i}\right)^2 \qquad \textbf{Equation 2.9}$$

where W_i is the data weight, d^{Calc} is the calculated data, and d^{Meas} is the measured data. When the L2-norm reduces to unity (1.0) or lower, the inversion is converged. The resistivity model is updated and the new inverted resistivity distribution is obtained. Forward modeling, using the updated model is performed in the next iteration to obtain calculated resistivity. This procedure is repeated until a new RMS error and L2-norm between the predicted data and the measured data criteria is satisfied. Otherwise, the stop criteria described in Chapter 3 - is modified and the procedure for inversion of resistivity measurements is repeated until inversion stop criteria is satisfied. For example, Figure 2.10 shows the results of an ERT survey performed at site one following the procedure described previously for inverting measured apparent resistivity. The inverted resistivity section converged in three iterations, had a root mean squared error of 3.47%, and an L2-norm of 0.94. All desired criteria (described below) were met and the inverted resistivity section accurately represented the true subsurface image.

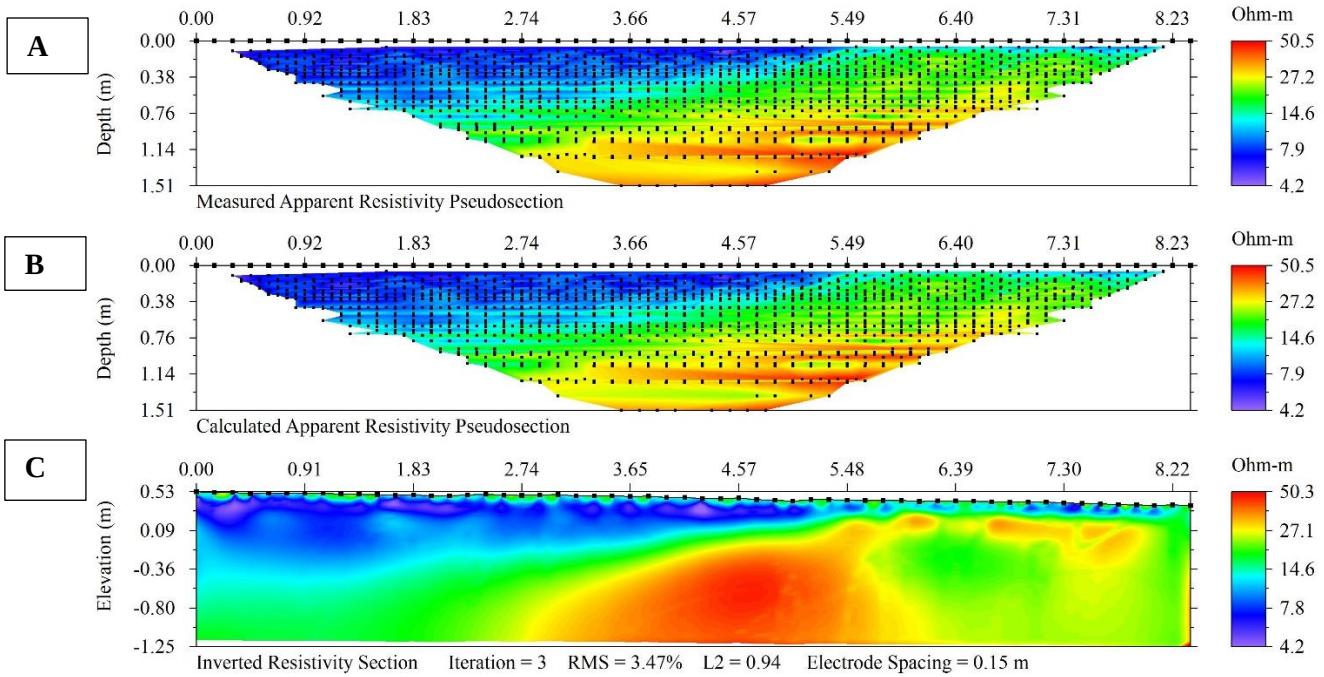

Figure 2.10. Example of inversion of an ERT survey performed at site one: A) Measured data collected in the field; B) Calculated apparent resistivity with forward modeling; C) Final inverted resistivity section converged after three iterations; RMS = 3.47%; L2-Norm = 0.94.

In this research, the goal is to obtain an RMS less than five percent, an L2-norm close but not exceeding unity (1.0), and no more than five iterations to achieve an inverted ERT section which accurately represents the true resistivity of the subsurface. All final inversions met the stop criteria and indicated excellent or good agreement between measured and calculated resistivity according to Tucker et al. (2015).

Factors affecting subsurface electrical resistivity

Soil type. The soil type (i.e., particle size distribution and mineralogy) is correlated with the measured electrical resistivity. Figure 1.1 shows the typical range of electrical resistivity for earth materials. Electrical resistivity measurements are the reciprocal of electrical conductivity (EC) measurements. EC measurements are dependent on the electrical charge density at the surface of solid constituents. Higher electrical charges are associated with clay particles and lead to high EC measurements and low electrical resistivity measurements (Fukue et al., 1999). Conversely, coarse-grained soils (i.e., sands and gravels) have larger voids than fine-grained soils and lead to very low EC measurements and high electrical resistivity measurements. A study conducted on 25

different clay samples found the electrical resistivity measurements ranged from 1 to 12 Ohm-m (Giao et al., 2003); conversely, electrical resistivity measurements for sand were variable depending on water content and ranged from 20 to 200 Ohm-m (Everett, 2013).

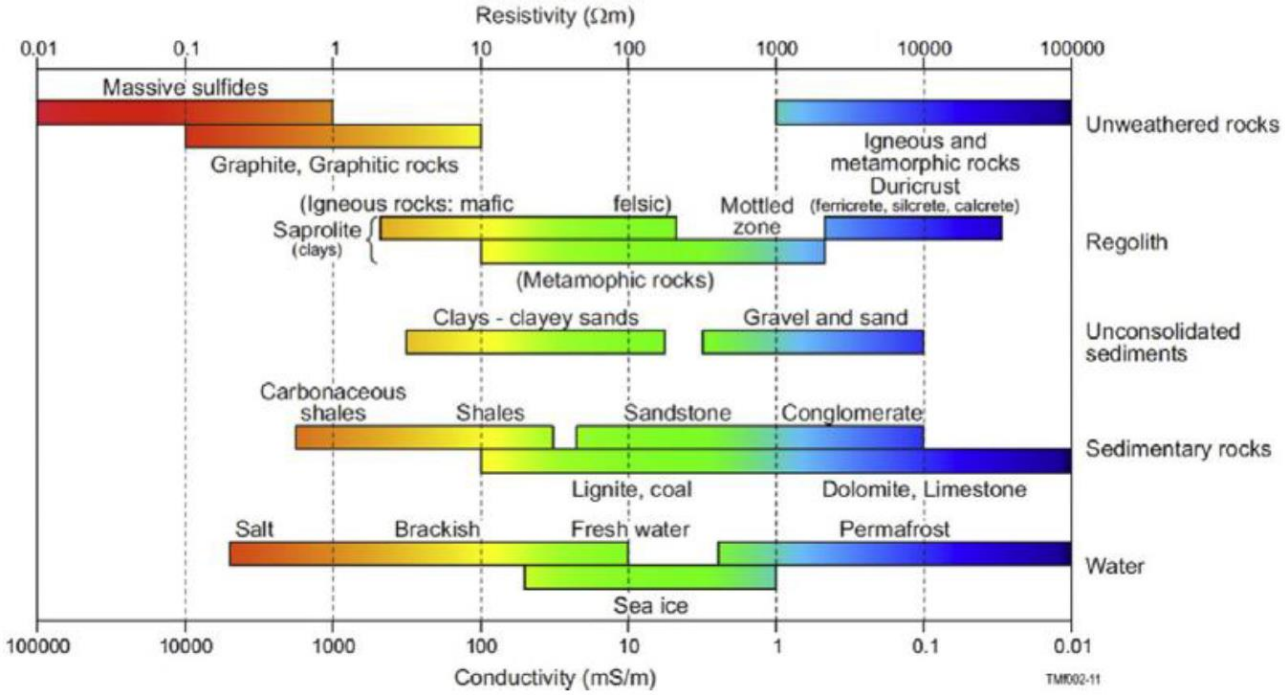

Figure 2.11. Typical ranges of electrical resistivities of earth material. (Palacky, 1987)

Abu-Hassanein et al. (1996) found a relationship between the liquid limit and plasticity index and the electrical resistivity on ten compacted clay samples (A, B, C, D, E, F, G, H, I, J). Figure 2.12 shows the electrical resistivity plotted versus the liquid limit and plasticity index for the samples with a liquid limit ranging from 23 to 70 and a plasticity index ranging from 5 to 46. The results from this study indicated a trend of higher liquid limit and plasticity index yielding lower electrical resistivity values. However, sample C did not fit this trend even though high liquid limit and plasticity index were determined for the sample which passed the No. 4 sieve. Therefore, only the soil passing the No. 200 sieve was used to determine the electrical resistivity for sample C. As a result, the sample C was consistent with electrical resistivity of the other soils having similar liquid limit or plasticity index.

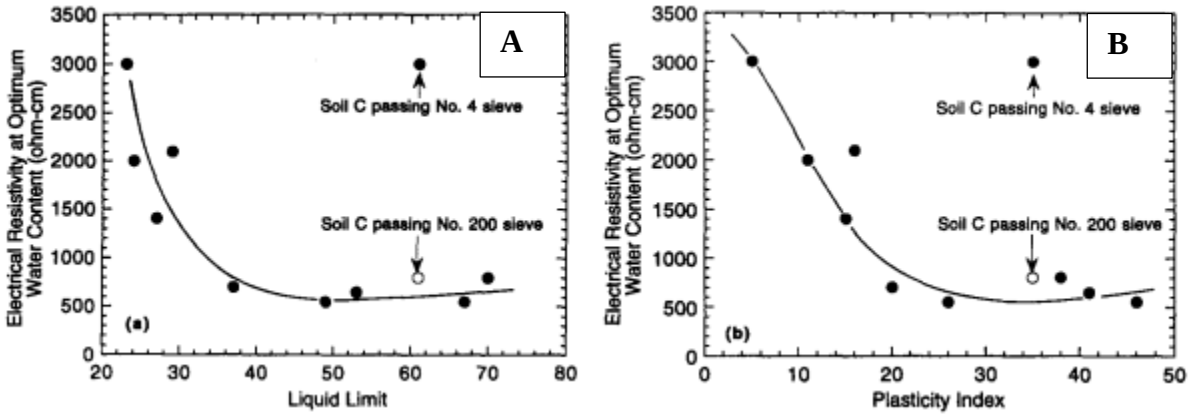

Figure 2.12. Relationship between electrical resistivity: (A) Liquid limit; (B) Plasticity index. (Abu-Hanssanein et al., 1996)

The electrical resistivity was also correlated to the percent of fines and coarse fracture of soils. Using the same ten clay samples (A, B, C, D, E, F, G, H, I, J) previously mentioned, Abu-Hanssanein et al. (1996) found that by increasing the percentage of fines a lower electrical resistivity measurement was obtained (Figure 2.13(A)). Soils with higher percent of fines generally have a higher specific surface, which improves surface conductance (Kwader, 1985; Abu-Hanssanein et al., 1996). Conversely, increasing the percentage of coarse fraction resulted in a higher electrical resistivity measurement (Figure 2.13(B)). Keller and Frischknecht (1996) attributed this behavior to the coarse fracture soil containing primarily quartz and feldspar which have high electrical resistivity.

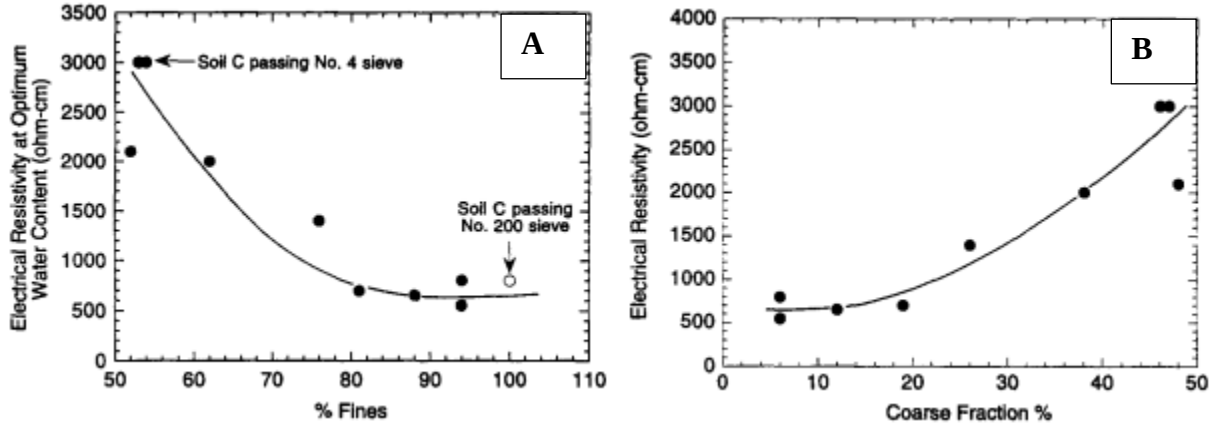

Figure 2.13. Relationship between electrical resistivity: (A) Percentage fines; (B) Coarse fraction percentage. (Abu-Hassanein et al., 1996)

Soil water content. Kibria and Hossain (2012) correlated soil electrical resistivity to the gravimetric water content of four clay samples. This study was performed using gravimetric water contents that varied between 10 and 50% while keeping the dry unit weight constant. In Figure 2.14, the results indicated that soil electrical resistivity in all samples decreased with increasing gravimetric water content up to approximately 20%. The average soil electrical resistivity reduction was 13.8 Ohm-m for change in gravimetric water content from 10 to 20%. The soil electrical resistivity was affected at gravimetric water contents less than 40%. Minimal variation in soil electrical resistivity was observed at 50% gravimetric water content between the four samples.

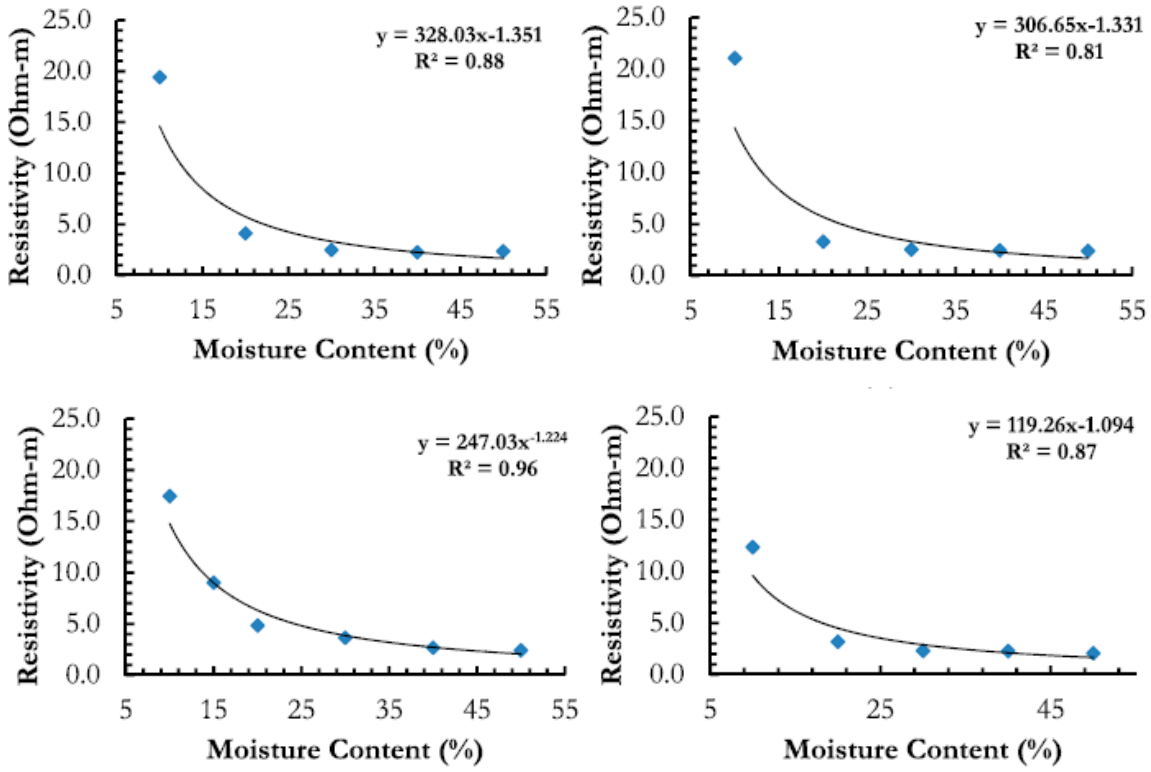

Figure 2.14. Relationship between electrical resistivity and gravimetric water content. (Kibria and Hossain, 2012)

Soil unit weight. The correlation between electrical resistivity and moist unit weight was developed by Kibria and Hossain (2012) using the same four clay samples shown in Figure 2.14. In this study, electrical resistivity tests were conducted at different moist unit weights while keeping the gravimetric water content constant. In Figure 2.15, the electrical resistivity was plotted for the four samples at a gravimetric water content of 18%. The results from this study indicated

that soil electrical resistivity decreased as the moist unit weight increased. Minimal change in soil electrical resistivity was observed after 15.72 kN m^{-3} in the four samples, which was likely caused by flocculated fabric breakdown at a high unit weight and reduction in the current flow path (Kibria and Hossain, 2012). According to Mitchell and Soga (2005), reduction in large pores and breakdown in flocculated open fabric occurs during the remolding of clay soil. As result, the conduction path in the soil reduces at a high unit weight.

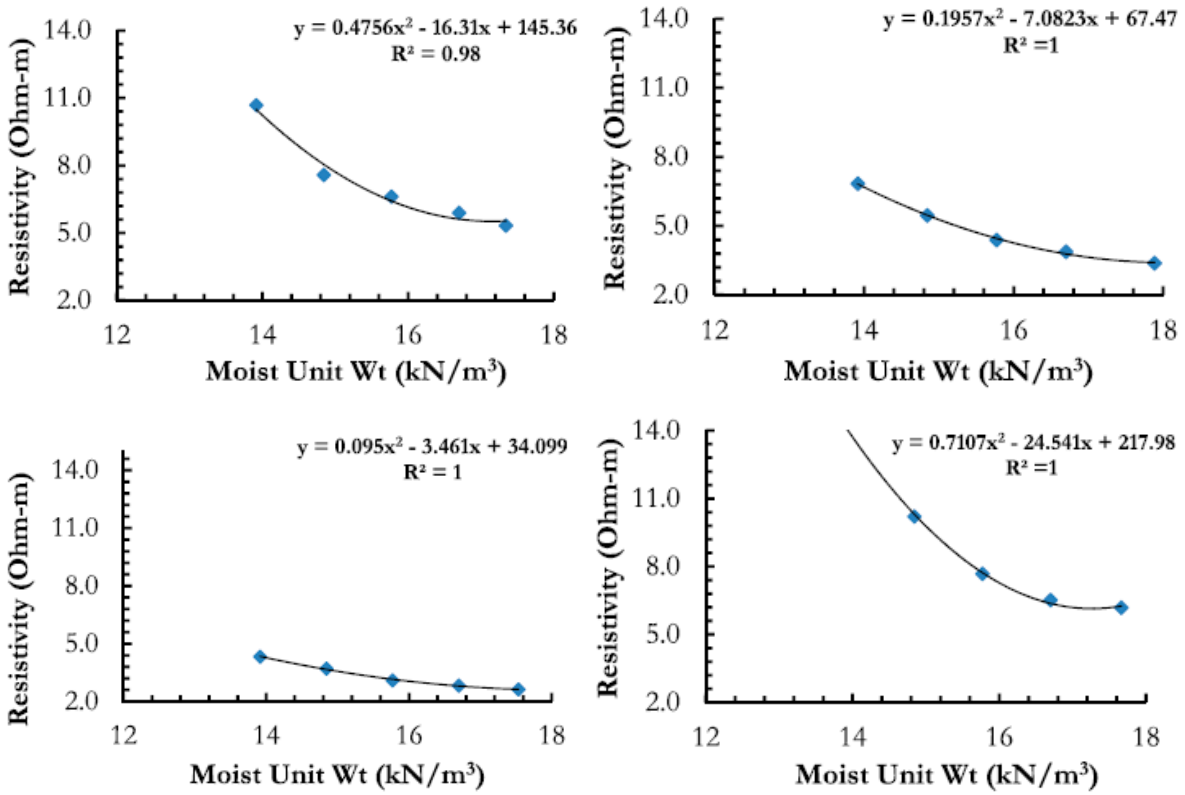

Figure 2.15. Relationship between electrical resistivity and moist unit weight. (Kibria and Hossain, 2012)

Chapter 3 - Methodology

3.1 Overview

This section includes the research methodology for this project including field and laboratory work. In order to determine the spatial variability of the claypan layer, ERT surveys were conducted in a high electrical conductivity area moving towards a low electrical conductivity area as measured with a surface conductivity mapper. Two field locations with identical land management practices were tested. Soil sample locations were determined using the ERT data. Undisturbed samples were used to preform erosion, strength, and permeability tests. Grab samples were used for soil classification.

3.2 Site description

Two agricultural sites near Bartlett, KS were selected in collaboration with the land owner for this research. Site one is 44.5 ha and site two is 30.8 ha. Sites one and two are approximately 1 km from each other and were converted from conventional tillage to no-tillage in the past 10 years. Sites one and two are shown in Figure 3.1.

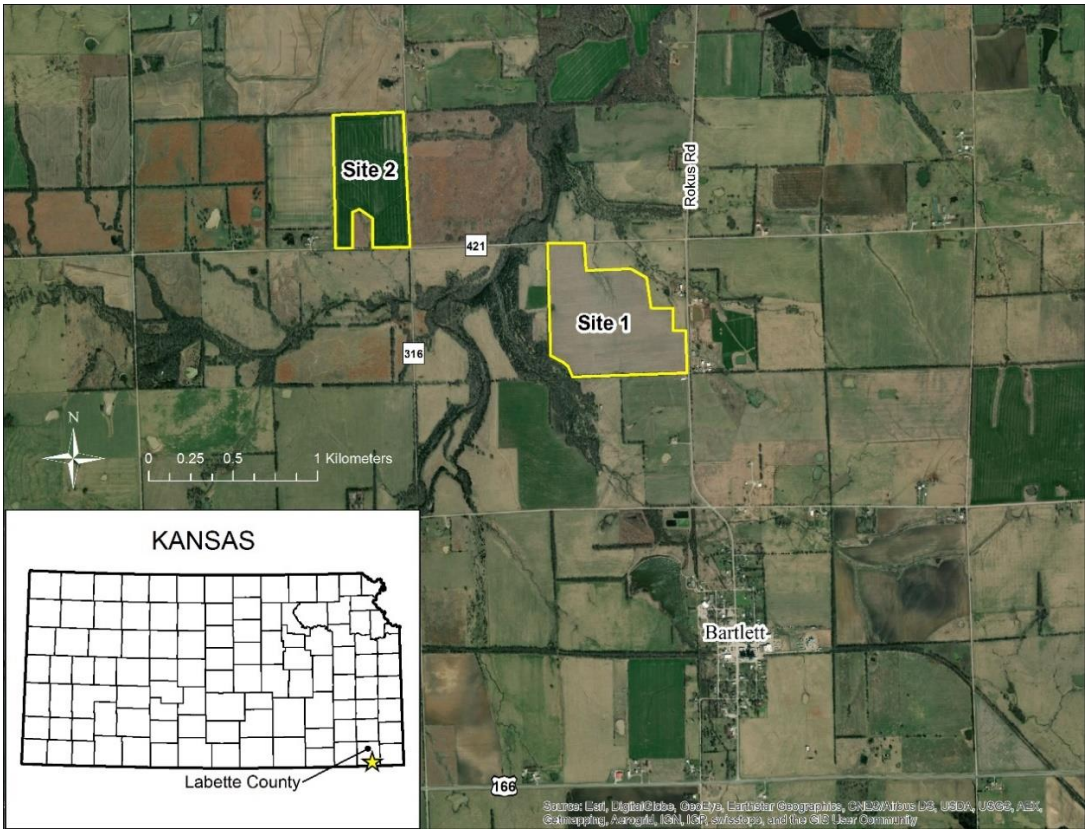

Figure 3.1. Regional and local location of sites one and two.

3.3 Geophysical methods

Apparent electrical conductivity (EC_a). The goal of mapping the apparent electrical conductivity (EC_a) was to determine the relative soil property variability across both sites. A Veris model 3100 sensor cart system (Veris Industries, Salina, KS), in concert with a global positioning system mounted on a tractor was used to measure the EC_a (Figure 3.2(A)). The system used six 43 cm diameter disc electrodes that remain in direct contact with the soil at an approximate depth of 6 cm (Figure 3.2(B)). Similar to ERT surveys discussed in Chapter 2, the Veris 3100 system used two discs that served as the current/sink and the remaining two-disc electrodes measured the resulting voltage potential. The disc spacing of 30 cm was used because this was the depth of interest for this study based on regional knowledge. Data processing was not needed for this test because due to the shallow depth of measurement, the representative volume of soil in each EC_a measurement is statically homogenous within the spatial resolution of surface EC_a mapper (Friedman, 2005). The EC_a measurements were mapped in SMS Advanced (AgLeader, Ames, IA). Boundary conditions were determined using the EC_a map and corn yield map at both sites. High EC_a and low corn yield indicated a claypan layer was likely near the surface and was designated a "high EC_a" area. Low EC_a and high corn yield indicated there was likely no claypan layer near the surface and was designated a "low EC_a" area. An area of interest was determined from the EC_a map and corn yield map of both sites and ERT surveys were performed in these locations.

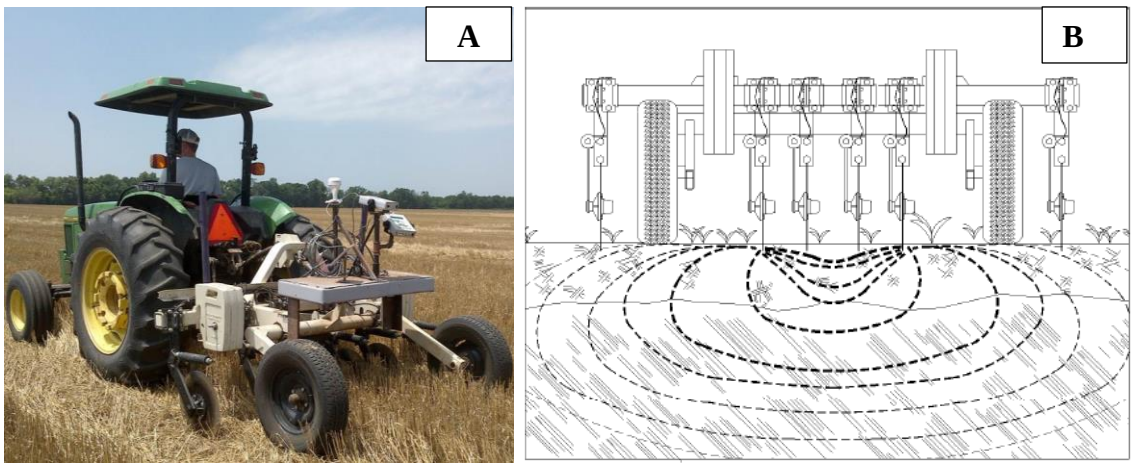

Figure 3.2. Electrical conductivity testing: (A) Tractor mounted Veris 3100 system used to measure the EC_a. (B) Schematic of Veris 3100 mapping system (Lund and Christy, 1998).

Electrical resistivity tomography (ERT). The goal of the ERT surveys were to determine the soil stratigraphy and soil sample locations at both sites. ERT surveys were conducted moving from an area where there was likely a claypan layer near the surface (i.e., high EC_a area) to an area where the claypan layer was likely not near the surface (i.e., low EC_a area).

An Advanced Geosciences Inc. (AGI) 'SuperSting with Wi-Fi Eight-Channel Earth Resistivity, Induced Polarization and Self Potential Instrument for Geo-Electrical Tomography' (SuperSting) meter was used to collect all ERT data. The SuperSting recorded up to eight voltage reading per single current injection which reduced the data collection time. There were 14 cables with four stainless steel electrodes per cable allowing for an ERT survey with 56 electrodes. Each stainless-steel electrode was fastened to a 30 cm long, 20 cm diameter stainless steel stake. To ensure contact for the injection current, the stainless-steel stakes were driven into the ground so that the electrodes sat just above the ground surface. All debris, such as corn stalks, were removed from around each stainless-steel stake and stainless-steel electrode.

AGI's SuperSting Administrator was used to create a command file prior to going to the field. The command file settings allow the user to set the number of electrodes, spacing of electrodes, type of array (i.e., sequence of current injection), number of commands per readings, and approximate measurement time per electrode. Simulating the command file allows the user to determine an approximate survey depth and data collection time to optimize data collection. The command file is saved and loaded to the SuperSting.

The primary intention of ERT surveys was to delineate near-surface (i.e., less than 9 m) soil stratigraphy, so the criteria considered for the selection of array type included vertical and horizontal resolution. Vertical resolution mapped horizontal features which helped distinguish distinct soil layers. Horizontal resolution mapped vertical features which helped identify discrete soil features within soil layers. The strong gradient array was selected because it provided high vertical and horizontal resolution near the surface and minimized near-surface noise, which was useful in distinguishing near-surface soil stratigraphy (Butler, 2005). The strong gradient, a hybrid array, combined the Dipole-dipole and inverted Schlumberger arrays, as discussed in Chapter 2 - .

A 56 electrode ERT survey line with an electrode spacing of 15 cm or 31 cm was used at both sites (Figure 3.3(A)). All ERT surveys were setup in such a way that the midpoint of the one ERT survey was the starting point of another ERT survey (Figure 3.3(B)) or the end of one ERT

survey was the starting point for another survey (Figure 3.3(C)). The red dashed line in Figure 3.3 (B-C) indicates the areas of interest determined from the EC_a map and corn yield map at both sites. The ERT surveys began in a high EC_a area and ended in a low EC_a area for both sites. A tape measure was used to determine placement of each stainless-steel stake. The stainless-steel stakes were driven into the ground with a hammer at a predetermined electrode spacing and the electrodes were fastened to the stainless-steel stakes. The cables adjacent to the 28th and 29th electrodes were connected to the SuperSting. Two 12V DC batteries were used to power the SuperSting. After completing setup, a contact resistance test was performed to ensure each stainless-steel electrode was properly fastened to each stainless-steel stake. The data collection time for each ERT survey using a strong gradient was approximately one hour. Terrain analysis was conducted using a Total Station surveying system to record the ground-surface elevation at each stainless-steel electrode. A terrain file was created from the recorded relative elevation values and utilized for post processing of the ERT survey data. ERT data collected from each survey was processed using AGI's EarthImager 2 ware.

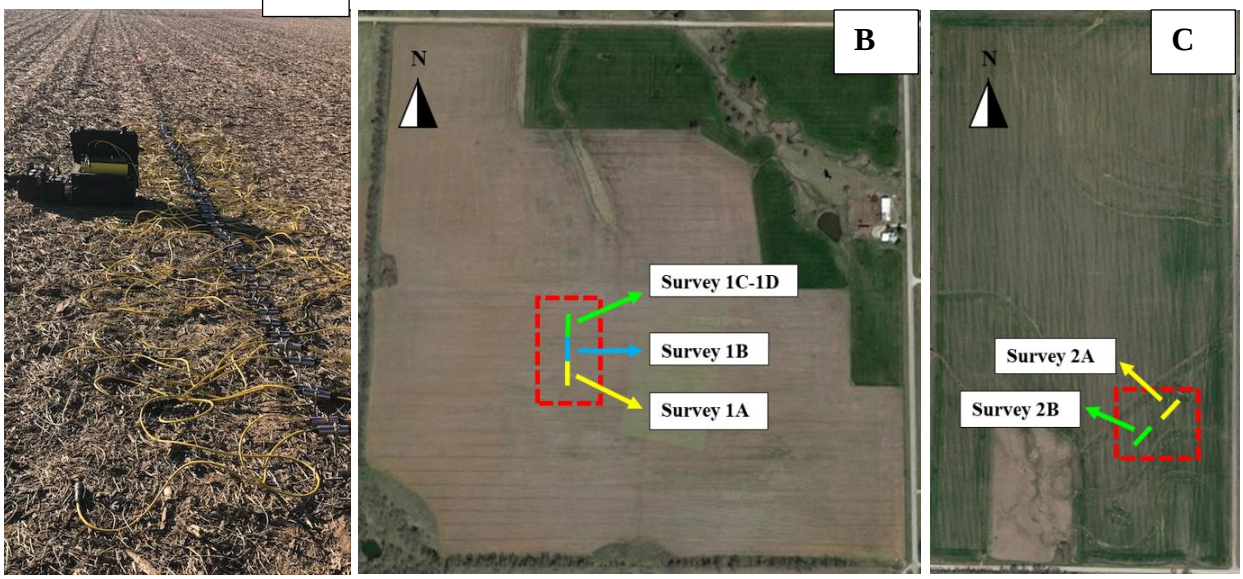

Figure 3.3. ERT experimental setup: (A) ERT survey line; (B) Site one ERT survey location; (C) Site two ERT survey location.

Data processing. All ERT data were processed using AGI's EarthImager 2D software to determine the true resistivity distribution in the subsurface. Initial settings criteria for data removal used for the processing of all ERT data included removal of negative apparent resistivities, removal of anomalous and singular spikes on the apparent resistivity pseudosection, a minimum voltage of 0.2 mV, a minimum voltage measurement normalized by the injected current of 0.0001 Ohm, a

minimum apparent resistivity of 0.1 Ohm-m, and a maximum apparent resistivity of 100,000 Ohm-m. These criteria were selected to remove noisy data and improve the data inversion.

A Smooth Model inversion method was selected for all ERT data processing. Forward modeling settings were chosen after selecting the initial settings criteria. A Finite Element Method utilizing the Cholesky Decomposition Method equation solver and a mixed boundary condition were used for all forward models. Resistivity inversion settings for all ERT data included the following stop criteria: a maximum of eight iterations, a maximum root mean squared (RMS) error of 5%, and using the L2-norm criteria. The following data weight criteria were selected: use of reciprocal error, and suppression of noisy data.

3.4 Soil sampling

Sample collection procedure. Soil sample locations were determined from the ERT sections. Undisturbed and disturbed soil samples were collected where ERT sections indicated a claypan layer was likely near the surface (i.e., high EC_a area) and not (i.e., low EC_a area). All soil samples were collected via a direct push method using a tractor mounted Giddings soil sampler (Giddings Machine Comp, Windsor, CO). The sampler was left in the ground a minimum of ten minutes to ensure there was no sample disturbance and to maximize push recovery. The undisturbed soil samples' collection depth was between 30 and 72 cm. Undisturbed soil samples were used to perform strength, erosion, and permeability tests. The disturbed samples were collected using 7.6 cm in diameter and 91 cm long plastic tubes. Disturbed soil samples were used to perform soil classification tests.

After sample collection, all soil samples were sealed at both ends using plastic or rubber end-caps. Duct tape was used to seal the end-caps to the soil sample tube. This was done to preserve in-situ water content of each soil sample until sample storage. All soil samples were labeled with the site number and sample location. Upon returning to the university, all soil samples were stored in a 100% humidity-controlled room until performing laboratory tests. A field log of soil samples collected at each site was created and recorded the following: the inverted ERT section containing the soil sample, the location of the soil sample within the inverted ERT section, the type of sample collection, the type of sample, the test preformed on the soil sample, the sample depth, and initial water content.

3.5 Erosion test methods

Erosion function apparatus (EFA). The goal of the EFA test was to directly measure the erosion rate and critical shear stress due to sheet flow erosion. The EFA, shown in Figure 3.4, consists of the following: flow straightener, water flow pump, piston advancing motor, piston, and flow sensor.

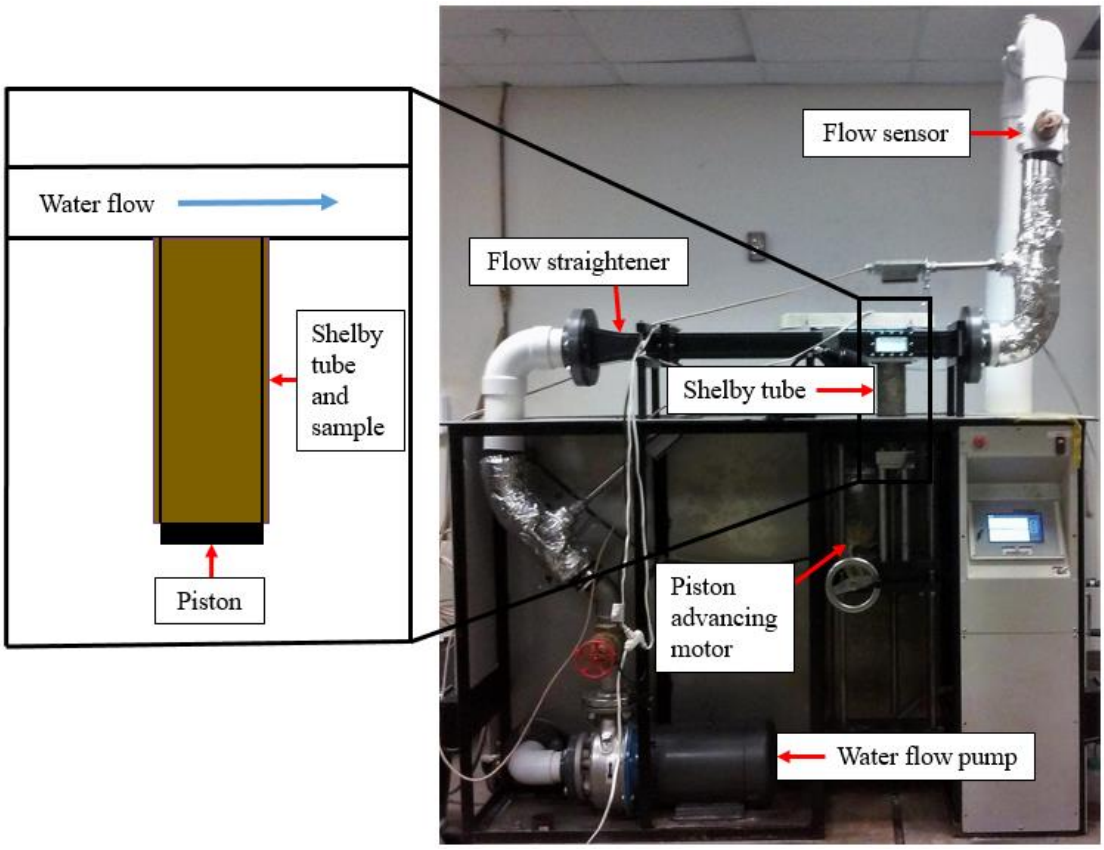

Figure 3.4. Schematic of KSU-EFA

Prior to testing, the water content of each undisturbed soil sample was measured according to ASTM D2216-10 (ASTM, 2010). The Shelby tube containing the undisturbed soil sample was placed on the EFA piston platform. All Shelby tube samples where 8 cm in diameter and 30 to 38 cm in length. The top portion of the sample was trimmed level with the Shelby tube and the sample was inserted into the opening of the flume by raising the platform using a crank wheel.

All samples were tested for one hour at six different velocities ranging from 1.0 to 6.0 m/s, in 1 m/s increments. At test initiation, the top of the sample was set flush with the bottom of the flume and the velocity was set at 0.5 m/s and increased to 1 m/s for the first velocity by pressing the flow button on the interactive LCD screen. As soil eroded from the Shelby tube, the piston was

pushed to ensure the sample was kept flush with the top of the Shelby tube and bottom of the flume. During testing, the velocity and amount of pushing by the piston was monitored and recorded continuously. After each velocity, a photo of the soil surface was taken (e.g., Figure 3.5) and processed using the custom photogrammetry computational program to quantify the surface roughness for determining the applied hydraulic shear stress (as described by Tran et al. (2017)). Prior to testing at the next velocity, the top portion of the sample was trimmed level to the Shelby tube and bottom of the flume.

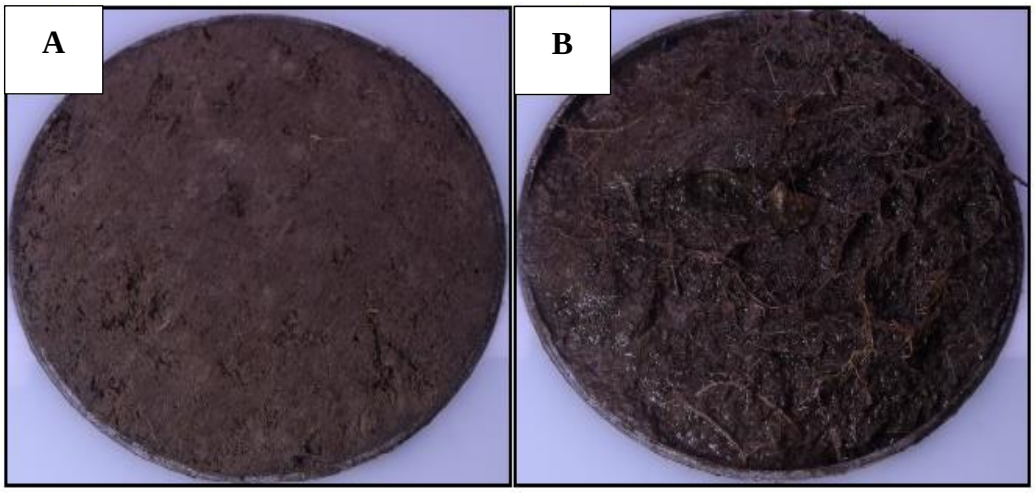

Figure 3.5. EFA soil sample surface: (A) Before testing; (B) After testing (Tran, 2018).

Data processing. The EFA data analysis determines the erosion rate and the applied hydraulic shear stress on the surface of the sample at each velocity. The erosion rate at each flow velocity was calculated as:

$$\dot{z} = \frac{h}{t} \qquad \textbf{Equation 3.1}$$

where $\dot{z}$ is the erosion rate (mm hr^{-1}), h is the length of sample eroded (mm), and t is the testing time at each velocity (hr). The applied hydraulic shear stress, determined from EFA testing, was calculated as:

$$\tau = \frac{1}{8} f \rho v^2 \qquad \textbf{Equation 3.2}$$

where τ is the shear stress on the sample surface (Pa), f is the friction factor obtained from the Moody chart (Moody, 1944) using the soil roughness, ρ is the mass density of water (kg m^{-3}), and v is the flow velocity (m s^{-1}). These data were used to create a plot of erosion and shear stress for each sample.

“Mini” jet erosion test (JET). The JET was performed at the surface and directly on the claypan layer (i.e., approximately 25 cm below the surface) at both sites to determine the erosion rate of the soil layers. The JET apparatus (Figure 3.6) consists of the following parts: water inlet, rotatable plate (containing the jet nozzle and gauge depth), jet nozzle, depth gauge, submergence tank, foundation ring, and water outlet. The jet nozzle is 3.18 mm in diameter and the submergence tank is 70 mm in height with a wall thickness of 6.4 mm. The foundation ring is 180 mm in diameter and 51 mm in height.

All JET locations were determined based on results from the ERT sections. The JET foundation ring was driven 51 mm into the soil surface using a rubber mallet to minimize soil disturbance. All debris (e.g., corn stalks) was removed from around the foundation ring. The submerged tank was attached to the foundation ring and the depth gauge was locked into place to ensure no surface soil disturbance prior to testing. An adjustable metal pipe containing the head tank was inserted through a metal tripod stand and set next to the JET testing location. Hoses that were 1.59 cm in diameter were attached from (1) the water supply tank to the water flow pump, (2) the water flow pump to the head tank, (3) the head tank to the JET apparatus water inlet, and (4) the excess flow ports back to water supply tank. Two excess flow ports were located near the top of the head tank to control the water level inside the head tank. The head tank was attached to the metal pole and adjusted within the metal tripod. The predetermined height was measured from the excess flow ports to the top of the submerged tank. All JETs were performed with a height between 2.08 m and 2.41 m based on known soil layers from classification of samples collected at both sites. A 1.59 cm diameter hose was attached to the water outlet and diverted the water from the submergence tank away from the testing area.

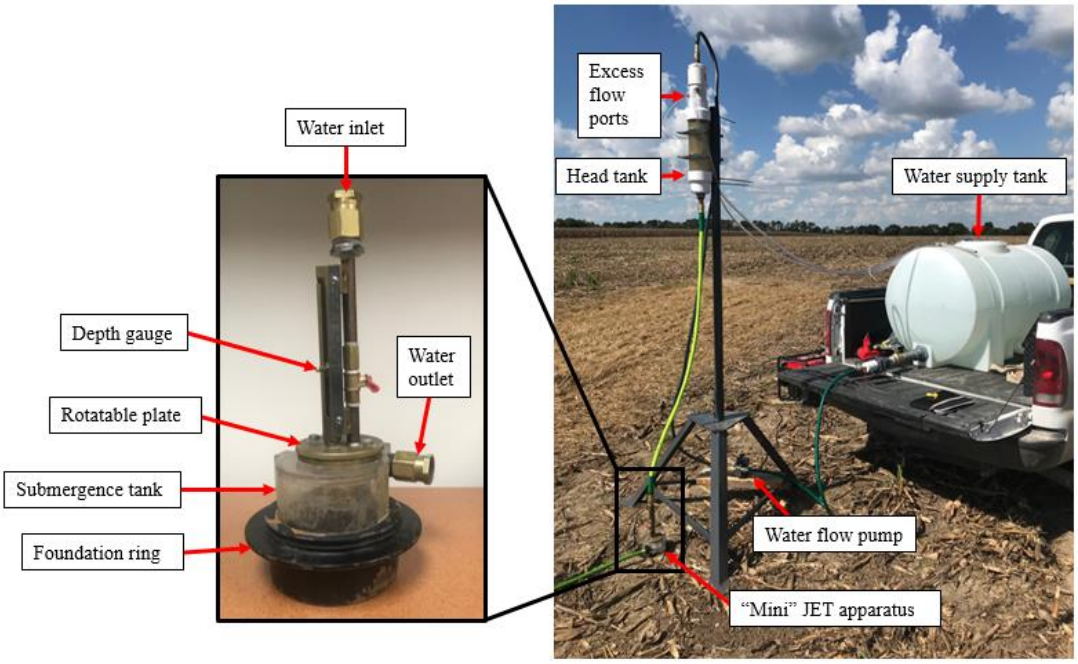

Figure 3.6. Schematic of the KSU-JET apparatus.

Next the initial depth to the surface was recorded at time zero. The submergence tank was filled with water to allow for soil saturation within the JET foundation ring. The jet nozzle was closed to protect the soil surface during initial filling of the submergence tank. Testing did not start until the submergence tank was completely filled and the water level in the head tank had reached a constant head. The head applied to the soil surface was measured from the excess flow ports to the top of the rotatable plate. At test initiation the jet nozzle was opened to allow the jet to directly impinge on the soil surface. Scour depth measurements were taken with the gauge depth while the impinging jet was closed. The scour depth was measured using a time interval according to the following: 5 seconds, 10 seconds, 15 seconds, 30 seconds, 1 minute, 2 minute, 3 minutes, 4 minutes, 5 minutes, 10 minutes, 15 minutes, 20 minutes, and 30 minutes. This time interval was selected to increase recorded scour measurements throughout testing. The time interval increased when the same scour depth measurement was recorded three times at the same time interval. For example, a scour depth of 49 mm was recorded three times using a 5 second time interval so the time interval was increased to 10 seconds. This measurement process was performed on all JETs with a maximum data collection time of two hours per test at both sites. All JET data were analyzed to determine the critical shear stress.

Data processing. The JET data analysis included determining the critical shear stress of soil at the surface and at the claypan layer. The following equations were used to estimate the

critical shear stress (Daly et al., 2013; Hanson and Cook, 2004). The critical stress was assumed to occur when the rate of scour was equal to zero at the equilibrium scour depth (Hanson and Cook, 1997) and was calculated as:

$$\tau_c = \tau_0 \left(\frac{J_p}{J_e}\right)^2 \quad \textbf{Equation 3.3}$$

where τ_0 is the maximum shear stress due to the jet velocity at the nozzle (Pa), J_p is the potential core length from the jet origin (cm), and J_e is the equilibrium scour depth (cm). The maximum shear stress was calculated as:

$$\tau_0 = C_f \rho_w U_0^2 \quad \textbf{Equation 3.4}$$

where C_f = 0.00416 is the coefficient of friction, ρ_w is water density (kg m^{-3}), and U_0 is the jet velocity at the orifice (cm s^{-1}). The velocity at the jet nozzle was calculated as:

$$U_0 = C\sqrt{2gh} \quad \textbf{Equation 3.5}$$

where C = 0.70 is the discharge coefficient, g is the gravity acceleration constant (cm s^{-2}), and h is the differential head measurement (cm). The potential core length from the jet origin was calculated as:

$$J_p = C_d d_0 \quad \textbf{Equation 3.6}$$

where C_d = 6.3 is the diffusion constant and d_o is the nozzle diameter (cm). To determine the equilibrium scour depth, Blaisdell et al. (1981) developed an equation which used the scour depth data versus time and a hyperbolic function. The general form of this equation is shown as:

$$A_1^2 = (f - f_0)^2 - x^2 \quad \textbf{Equation 3.7}$$

where A_1 is the value for the semi-transfer and semi-conjugate of the hyperbola, $f = \log(J/d_0) - x$, $x = \log[(U_0 t)/d_0]$, and $f_0 = \log(J_e/d_0)$. The coefficients A_1 and f_0 are determined by plotting f versus x. The equilibrium scour depth was calculated as:

$$J_e = d_0 10^{f_0} \quad \textbf{Equation 3.8}$$

All JET data analysis in this study used the scour depth solution.

3.6 Soil classification and parameters

The water content for each soil sample was determined before and after laboratory testing according to ASTM D2216-10 (ASTM, 2010). Most of the samples that were not collected in Shelby tubes visually contained two layers with distinctly different soil characteristics. These samples were collected in clear plastic tubes that did not maintain the in situ structure. The soil properties were measured for each layer (i.e., Top (T) of sample and Bottom (B) of sample) where

two layers were observed. All disturbed soil samples were classified according to the Unified Soil Classification System (USCS), ASTM D2487-17 (ASTM, 2018). The wet sieve analysis and dry sieve analysis were performed according to ASTM C117-17 (ASTM, 2017) and ASTM C136/136M (ASTM, 2015), respectively. Although not needed for classification, a hydrometer test was performed for all samples according to ASTM D7928-17 (ASTM, 2017). The Atterberg limits test was performed according to ASTM D4318-17e1 (ASTM, 2017). The undisturbed soil samples collected at both sites in Shelby tubes were taken within close proximity to the disturbed samples and were assumed to have the same soil classification corresponding to the nearest classified soil sample. The hydraulic conductivity test, ASTM D5084-16a (ASTM, 2016), and unconsolidated undrained triaxial compression test, ASTM D2850-15 (ASTM, 2015), were performed on the T and B portion of the undisturbed soil samples.

Chapter 4 - Results

4.1 Site one

Figure 4.1A shows the EC_a measurements of the upper soil layer measured at approximately 30 cm depth in the soil profile. High EC_a measurements from 65 to 109 µS cm^{-1} were observed in the center, highlighted by the dashed black rectangle. In Figure 4.1B, low corn yield measurements from 3,276 to 5,229 kg ha^{-1}, highlighted by the black dashed rectangle, directly correlated to the high EC_a area (Figure 4.1(A)). The solid black line in Figure 4.1(A) shows where the ERT surveys were performed moving from a high EC_a, low corn yield area to a low EC_a, high corn yield area.

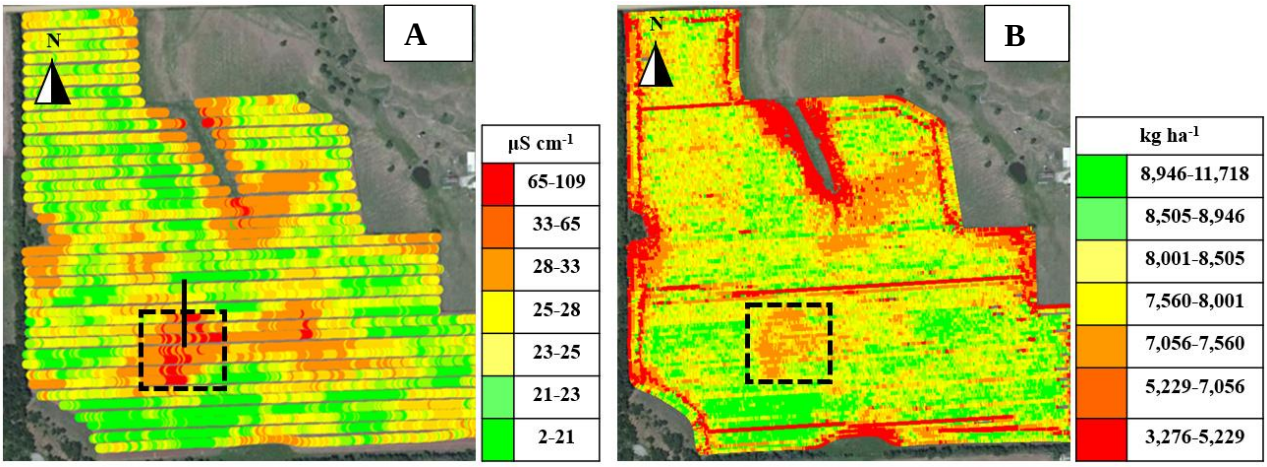

Figure 4.1. Site one: (A) Apparent electrical conductivity map measured with a VERIS system; (B) Corn yield map measured with a commercial yield monitor on a combine.

In Figure 4.2, four ERT surveys were performed moving from a high EC_a, low corn yield area (Surveys 1(A-B)) to a low EC_a, high corn yield area (Surveys 1(C-D)). An electrode spacing of 15 cm was utilized to identify the near-surface soil stratigraphy. The ERT surveys were performed such that the end of Survey 1A was the beginning of Survey 1B. This procedure was followed for the remaining ERT surveys. Electrical resistivity measurements in Survey 1A highlighted a low resistivity layer (10 Ohm-m or less), shown in purple, from the surface to -0.48 m below the surface. In Survey 1B, the transition area, the low resistivity layer (10 Ohm-m or less) thinned from 0.89 m to less than 0.31 m in thickness as the region measurements moved towards a low EC_a area. Electrical resistivity measurements in Surveys 1C-1D highlighted a thin low resistivity layer (10 Ohm-m or less) near the surface, however it is relatively thinner and appears to dissipate across the soil profiles compared to Survey 1A.

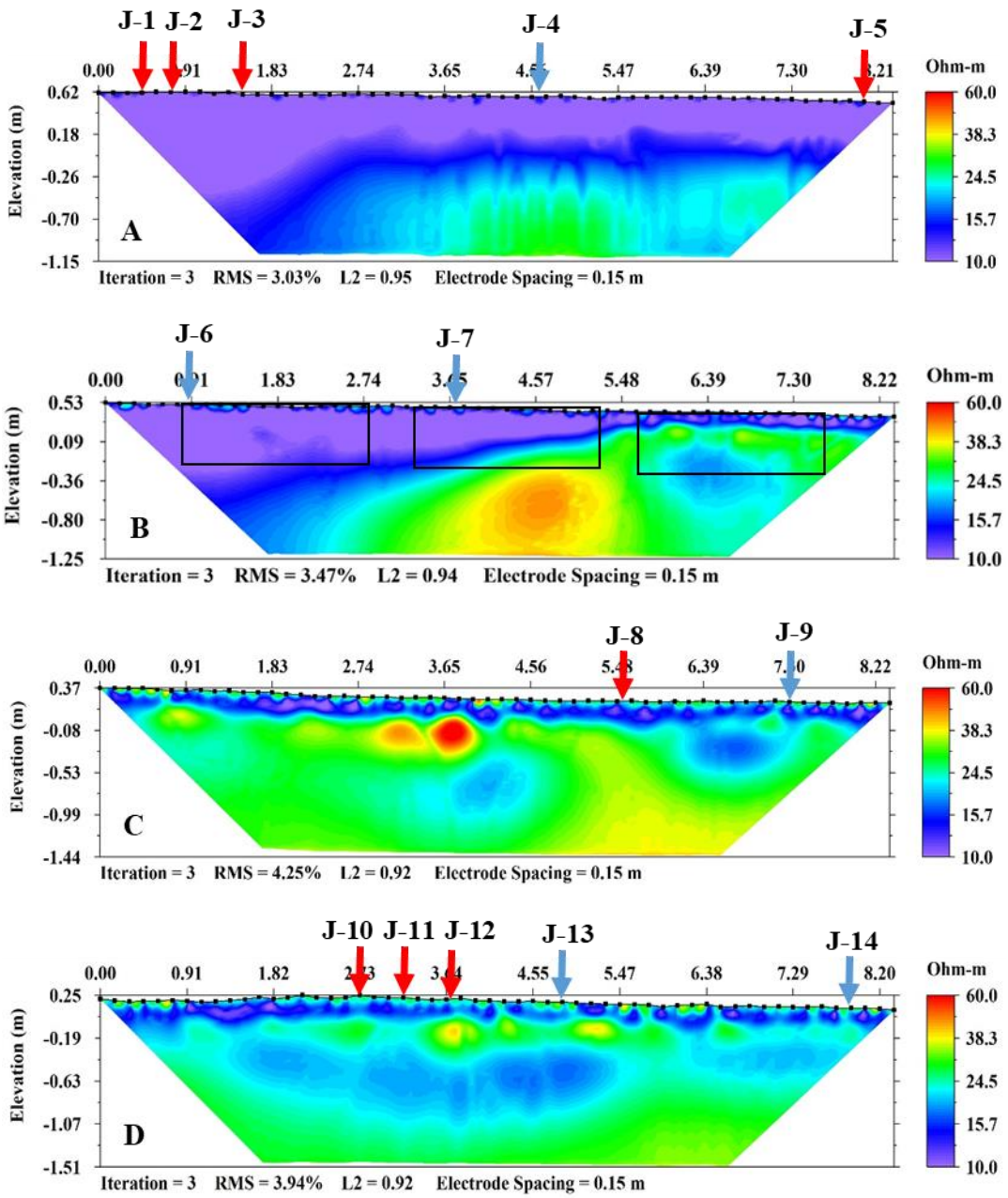

Figure 4.2. Site one ERT surveys: (A) Survey 1A; (B) Survey 1B; (C) Survey 1C; (D) Survey 1D. Blue arrows indicate the location of the JET surface tests, red arrows indicate the locations of the JET tests below the surface (~25 cm), black rectangles in 1B indicate location of soil sample collection.

Two layers were classified in the disturbed sample collected from Survey 1B. All top layers were classified as a lean clay (CL) and all bottom layers were classified as a fat clay (CH). The black rectangles (covering approximately 60 cm -120 cm) in Survey 1B show the area in which all

samples were collected. For example, all samples shown in Table 4.1 in the “low yield area” were collected within the black box shown on the far left of Figure 4.2(B). Samples 2 and 8 were used for undrained shear strength testing, Samples 2-2 and 8-2 (i.e., fat clay) had an undrained shear strength two times higher than Samples 2-1 and 8-1 (i.e., lean clay). Samples 3 and 9 were used for hydraulic conductivity tests, Samples 3-1 and 9 (i.e., lean clay) had a higher hydraulic conductivity than Sample 3-2 (i.e., fat clay). Sample 9, collected where there was no near-surface claypan layer, had a higher hydraulic conductivity than Sample 3-1, collected where there was a near-surface claypan layer. The EFA results from Samples 4, 6, and 10 indicated the lean clay layer had a relatively lower critical shear stress than the underlying fat clay layer. The EFA test was performed using undisturbed samples collected from Surveys 1B, note that is was not possible to obtain samples with two layers (i.e., top and bottom in Table 4.1) for all EFA samples.

Table 4.1. Site one soil parameters and erosion function apparatus results.

Area of Interest	Sample I.D.	Measurement Location	LL (%)	PI (%)	USCS	S_u (kPa)	K_{sat} (cm/s)	EFA Test
								τ_c (Pa)
Low yield area, near-surface claypan layer in Figure 4.2(B)	1-1	Top	30	14	CL	-	-	-
	1-2	Bottom	53	29	CH	-	-	-
	2-1	Top	-	-	-	47	-	-
	2-2	Bottom	-	-	-	103	-	-
	3-1	Top	-	-	-	-	2.2E-5	-
	3-2	Bottom	-	-	-	-	9.1E-7	-
	4	Bottom	-	-	-	-	-	118.26
Transition area in Figure 4.2(B)	5-1	Top	38	21	CL	-	-	-
	5-2	Bottom	73	52	CH	-	-	-
	6	Top	-	-	-	-	-	19.43
High yield area, no near-surface claypan layer in Figure 4.2(B)	7-1	Top	27	9	CL	-	-	-
	7-2	Bottom	76	51	CH	-	-	-
	8-1	Top	-	-	-	33	-	-
	8-2	Bottom	-	-	-	64	-	-
	9	Top	-	-	-	-	5.1E-3	-
	10-1	Top	-	-	-	-	-	18.73
	10-2	Bottom	-	-	-	-	-	74.49

Figure 4.3 shows the EFA results collected in a high EC_a area, the transition area, and low EC_a area at site one. Samples 4 and 10-2 were the least erodible, contained fat clay soil, and were classified as very low to low erodibility (Figure 4.3). Where possible, samples with two layers (i.e., CL overlying CH) were tested individually (i.e., upper and lower portion of the sample). There was no measurable erosion (via extrusion in the EFA) in Sample 4 until 6 m s^{-1} and Sample 10-2 did not erode until 5 m s^{-1}. In Figure 4.3, Samples 6 and 10-1 were more erodible, contained lean clay soil, and were classified as moderate erodibility. Measurable erosion was observed at 3 m s^{-1} in Samples 6 and 10-2, where the soil was classified as lean clay. Sample 10-1, collected where there was no near-surface claypan layer, was the most erodible; whereas, Sample 4, where

there was a near-surface claypan layer, was the least erodible. All erosion points were plotted according to HEC-18 erodibility categorization (Arneson, 2012), which does not show points corresponding to zero erosion rate as it is a log-log plot. Note that the critical shear stress in Table 4.1 was the shear stress that corresponded 0.1 mm/h erosion rate (Briaud et al. 2001). The EFA results for all samples are shown in Table 6.1 of Appendix A

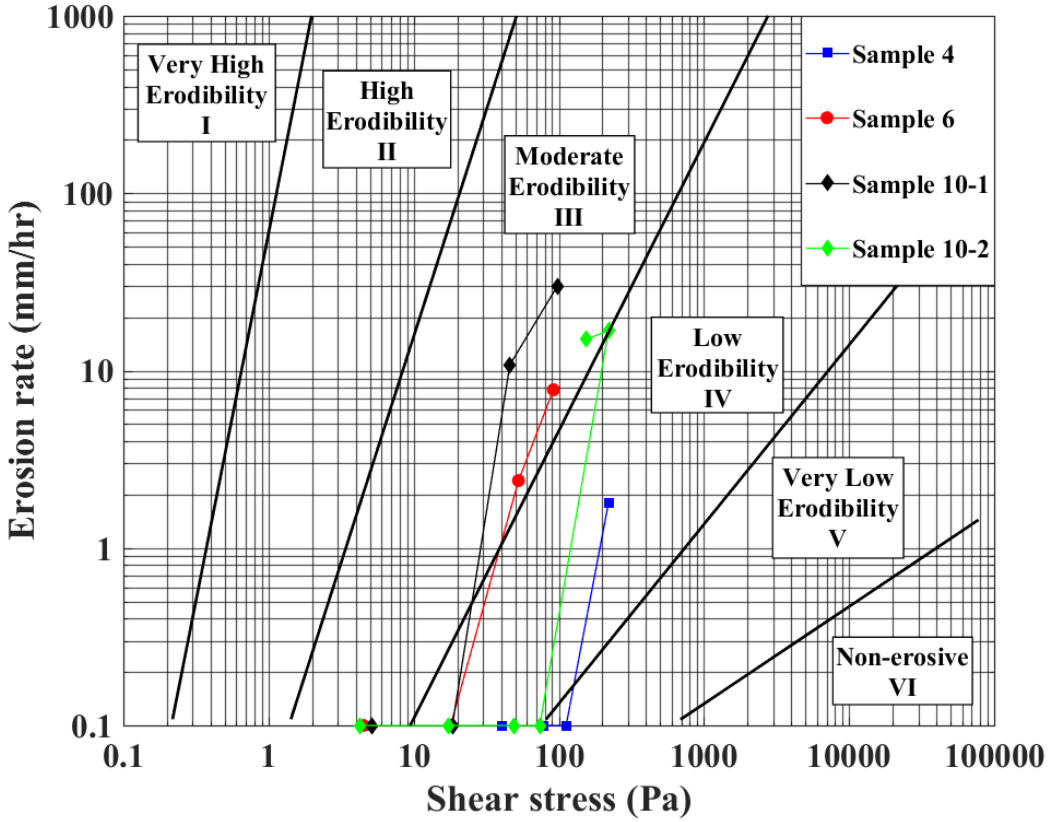

Figure 4.3. Site one EFA results for three sample locations.

Seven JET were performed in a high EC_a, low yield area (i.e., Surveys 1(A-B)) and seven in a low EC_a, high yield area (i.e., Surveys 1(C-D)). Six JET were performed at the surface, indicated by blue arrows in Figure 4.2, labeled as J-4, J-6, J-7, J-9, J-13, and J-14 in **Table 4.2**. Eight JET were performed approximately 25 cm below the surface, indicated by red arrows in Figure 4.2, labeled as J-1, J-2, J-3, J-5, J-8, J-10, J-11, and J-12 in Table 4.2. Where it existed, the claypan layer was assumed to be 25 cm below the surface. This assumption was validated based on the higher measured critical shear stress at 25 cm below the surface compared to the surface measurements as shown in Table 4.2. The critical shear stress determined for J-3 and J-8 were

erroneous and was not used to calculate the average critical shear stress. All JET data for determining the critical shear stress are shown in Tables 6.3, 6.4, and 6.5 of Appendix B.

Table 4.2. Site one jet erosion results.

Area of Interest	Location	Sample I.D.	Test Date	τ_c (Pa)	$\tau_{c,avg}$ (Pa)
Low yield area, near-surface claypan layer in Figure 4.2(A-B)	Surface	J-4	12/18/18	6.29	7.71
		J-6	12/18/18	6.80	
		J-7	12/18/18	10.03	
	25 cm Below Surface	J-1	10/17/19	16.75	15.54
		J-2	10/17/19	16.48	
		J-3	04/02/19	25.32	
		J-5	04/03/19	13.40	
High yield area, no near-surface claypan layer in Figure 4.2(C-D)	Surface	J-9	12/18/18	7.33	6.17
		J-13	12/18/18	5.05	
		J-14	12/18/18	6.13	
	25 cm Below Surface	J-8	04/03/19	12.00	7.10
		J-10	04/03/19	4.97	
		J-11	10/17/19	7.83	
		J-12	10/17/19	8.51	

The observed scour depth measurements closely correlated to the predicted scour depth method measurements (Figure 4.4). The Blaisdell method overpredicted scour at the claypan layer (i.e., Sample J-5) to be greater than 3 cm while scour depth method predicted a scour depth of less than 1 cm. The over-prediction of scour using the Blaisdell method verified the selection of the scour depth method to determine the critical shear stresses presented in Table 4.2.

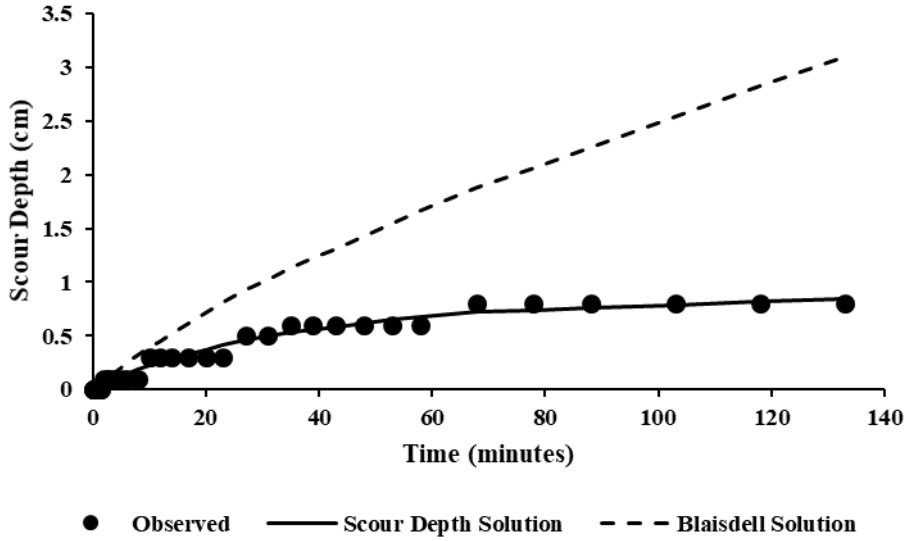

Figure 4.4. Site one JET observed and predicted scour depths on the claypan layer.

4.2 Site two

Figure 4.5(A) shows the EC_a measurements of the upper soil layer measured at approximately 30 cm in the soil profile. High EC_a measurements from 117 to 313 μS cm^{-1} were observed in the southeast portion of the site, highlighted by the dashed black rectangle. In Figure 4.5(B), low corn yield measurements from 1,260 to 4,473 kg ha^{-1}, highlighted by the black dashed rectangle, directly correlated to the high EC_a area (Figure 4.5(A)). The solid black like in Figure 4.5(A) shows where the ERT surveys were performed moving from a high EC_a, low corn yield area to a low EC_a, high corn yield area.

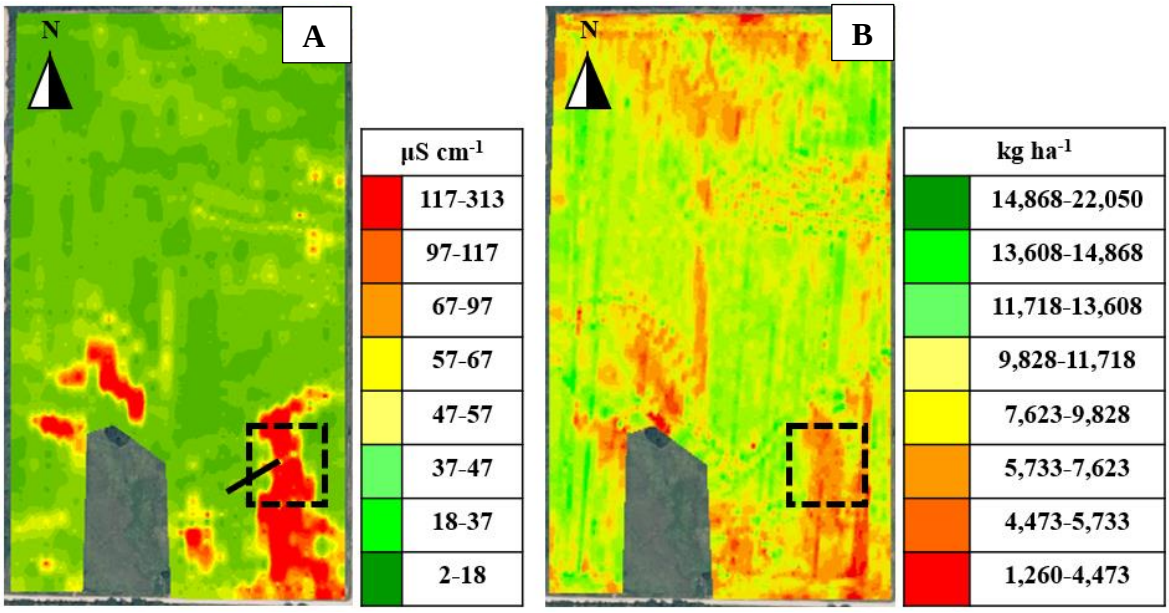

Figure 4.5. Site two: (A) Apparent electrical conductivity map measured with a VERIS system; (B) Corn yield map measured with a commercial yield monitor on a combine.

Two ERT surveys were performed moving from a high EC_a, low corn yield area (Survey 2A) to a low EC_a, high corn yield area (Survey 2B) (Figure 4.6). Unlike site one, an electrode spacing of 30 cm was selected to utilize a more efficient procedure for identifying the transition area while reducing the number of ERT surveys performed. Electrical resistivity measurements in Survey 2A highlighted a low resistivity layer (10 Ohm-m or less), shown in purple, from the surface to approximately -1.01 m below the surface with a thickness of 1.3 m. In Survey 2B, the ERT measurements highlighted a low resistivity layer (10 Ohm-m or less) with a thickness of 1.0 m at a depth of -0.30 m below the surface underlying a 0.5 m thick higher resistivity layer (15.7 Ohm-m or more). Survey 2B contained the transition area and a low EC_a area. The green dashed lines drawn in Survey 2B highlights the transition area. Unlike site one, the claypan layer does not appear to dissipate but rather it is found at a greater depth below the surface.

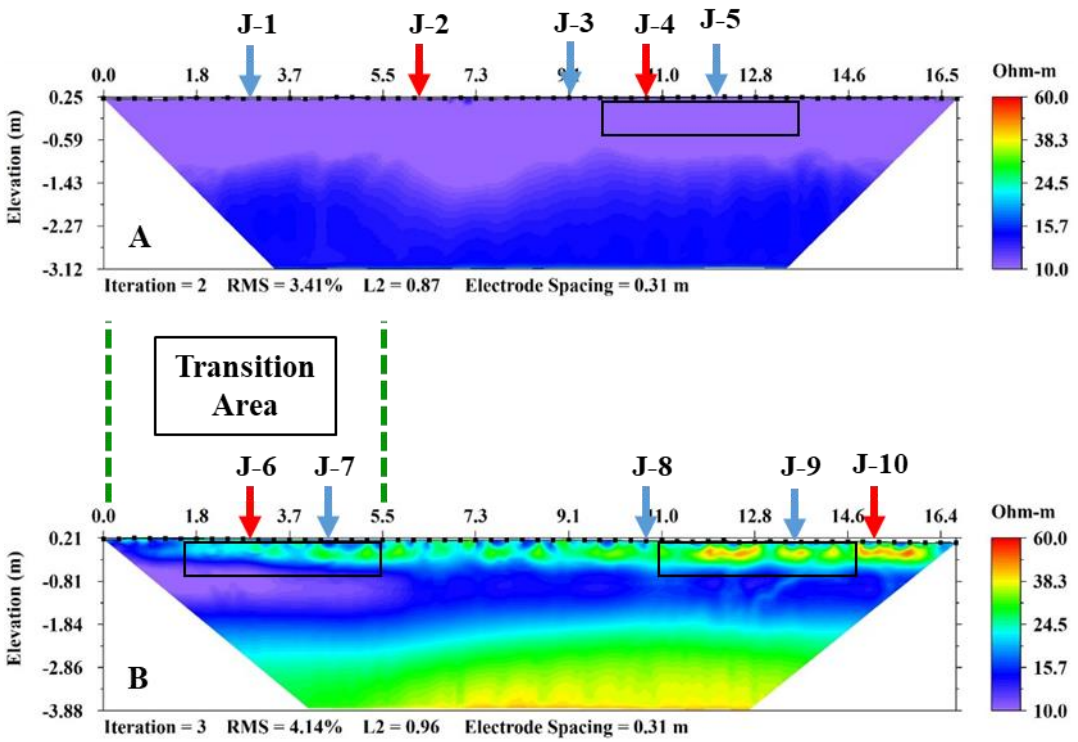

Figure 4.6. Site two ERT sections: (A) Survey 2A; (B) Survey 2B. Blue arrows indicate the location of the JET surface tests, red arrows indicate the locations of the JET tests below the surface (~25 cm), black rectangles indicate location of disturbed soil sample collection.

In Table 4.3, one layer was classified in Sample 1 (i.e., high EC_a area) and Sample 7 (i.e., low EC_a area) but Sample 5 (i.e., transition area) contained two layers (CL overlying CH). Samples 1 and 7 were classified as a lean clay (CL) soil according to the Unified Soil Classification System. Like site one, the black rectangles drawn in Figure 4.6(A-B) (covering approximately 60 cm -120 cm) show the location of all sample collection. For example, all samples shown in Table 4.3 in the "high yield area" were collected within the black box shown on the far right of Figure 4.6(B). Samples 2 and 8 were used for undrained shear strength testing, Sample 2-2 had an undrained shear strength two times higher than Sample 2-1; whereas, Samples 8-1 and 8-2 had similar undrained shear strength. Samples 3 and 9 were used for hydraulic conductivity tests and had relatively similar hydraulic conductivities. Sample 9, collected in the low EC_a area, had a higher hydraulic conductivity than Sample 3, collected where there was a near-surface claypan layer. The EFA results from Samples 4, 6, and 10 indicated the lean clay soil in the high EC_a area (i.e., Sample 4) was more resistant to erosion than the low ECa area (i.e., Sample 10) even though the soils were classified as a lean clay. This is evident by the relatively higher critical shear stress value for

Sample 4 and the relatively lower critical shear stress value for Sample 10 shown in Table 4.3. Note that is was not possible to obtain two layers (i.e., top and bottom in Table 4.3) for Sample 6 due to the depth of sample collection.

Table 4.3. Site two soil parameters and erosion function apparatus results.

Area of Interest	Sample I.D.	Measurement Location	LL (%)	PI (%)	USCS	S_u (kPa)	K_{sat} (cm/s)	EFA Test
								τ_c (Pa)
Low yield area, near-surface claypan layer in Figure 4.6(A)	1	Bottom	31	14	CL	-	-	-
	2-1	Top	-	-	-	28	-	-
	2-2	Bottom	-	-	-	60	-	-
	3	Bottom	-	-	-	-	1.7E-6	-
	4	Bottom	-	-	-	-	-	20.6
Transition area in Figure 4.6(B)	5-1	Top	28	10	CL	-	-	-
	5-2	Bottom	54	33	CH	-	-	-
	6	Top	-	-	-	-	-	5.52
High yield area, no near-surface claypan layer in Figure 4.6(B)	7	Top	30	11	CL	-	-	-
	8-1	Top	-	-	-	42	-	-
	8-2	Bottom	-	-	-	47	-	-
	9	Top	-	-	-	-	2.2E-5	-
	10	Top	-	-	-	-	-	5.34

Figure 4.7 shows the EFA results in a high EC_a, the transition area, and low EC_a area at site two. Previously noted, Sample 4, collected in a high EC_a area, was more resistant to erosion than Sample 10, collected in a low EC_a area, even though both samples were classified as a lean clay. Samples 6 and 10 were the least erodible and classified as moderate erodibility, whereas Sample 4 was the most erosion resistant to erosion and classified as low-moderate erodibility. Unlike Samples 6 and 10 which had no measurable erosion until 2 m s^{-1}, Sample 4 had no measurable erosion until 3 m s^{-1}. Sample 6, collected in the transition area, had a lower erosion rate than Sample 10, collected in a low EC_a area, at 2 m s^{-1} and 3 m s^{-1} flow velocity; however, at high water velocities (5 and 6 m s^{-1}), the erosion rates of Sample 6 were relatively higher than the erosion rate of Sample 10. Samples 4, 6, and 10 were more erodible than Sample 4, 6, 10-1, and 10-2 at site one. Like site one, all erosion points were plotted according to HEC-18 erodibility categorization (Arneson, 2012) and the critical shear stress in Table 4.3 was the shear stress that corresponded 0.1 mm/h erosion rate (Briaud et al. 2001). The EFA results for Samples 4, 6, and 10 are shown in Table 6.2 of Appendix A.

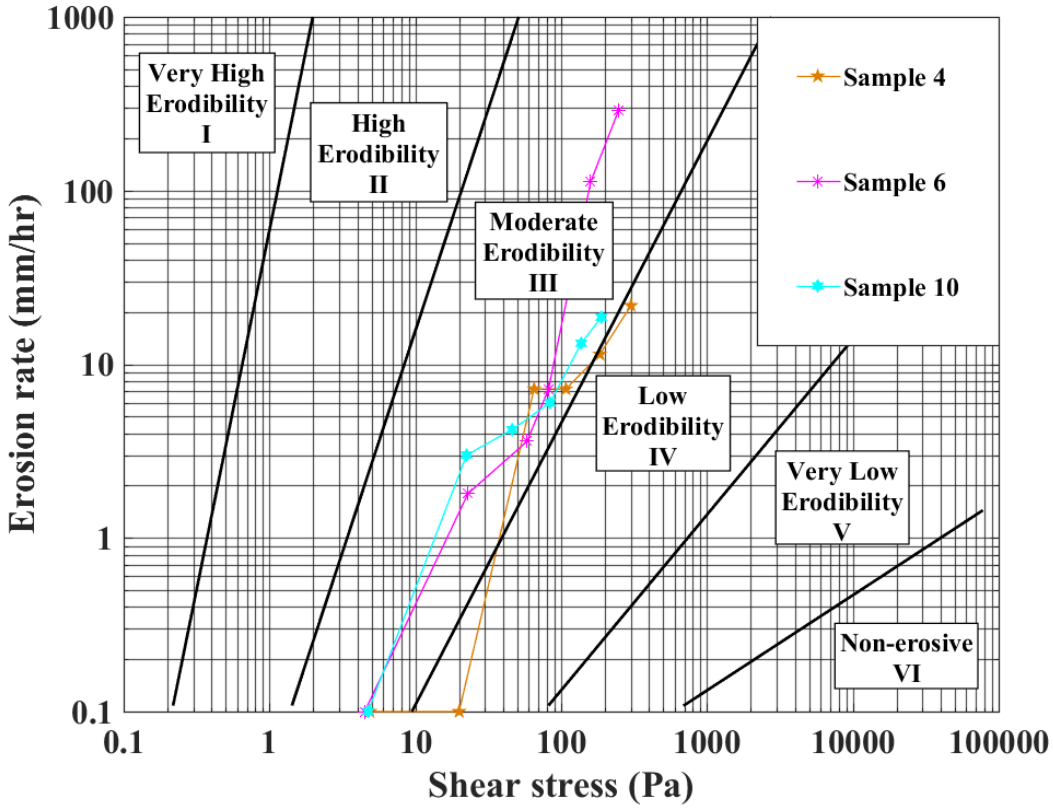

Figure 4.7. Site two EFA results.

Five Jet were performed in a high ECa, low yield area (i.e., Survey 2A) and five in a low ECa, high yield area (i.e., Survey 2B). Six JET were at the surface, indicated by blue arrows in Figure 4.6, labeled as J-1, J-3, J-5, J-7, J-8, and J-9 in Table 4.4. Four JET were performed approximately 25 cm below surface, indicated by red arrows in Figure 4.6, labeled as J-2, J-4, J-6, and J-10 in Table 4.4. Like site one, the claypan layer was assumed to be 25 cm below the surface where it existed. As expected, the critical shear stress at the surface was the same (within 1 Pa) between a high and low EC_a area indicating erodible soil at the surface. Unexpected, the critical shear stress 25 cm below the surface was also the same (within 2 Pa) between a high and low EC_a area. This indicated a more erosion resistant soil 25 cm below the surface. This was unlike site one where testing went to a clearly non near-surface claypan area. As discussed further in **Error! Reference source not found.**, it was likely that JET did not extend into an area where there was no claypan. These results support a claypan layer underlying both a high and low EC_a area. All JET data for determine the critical shear stress are shown in Tables 6.6, 6.7, and 6.8 of Appendix B.

Table 4.4. Site two jet erosion results.

Area of Interest	Location	Sample I.D.	Test Date	τ_c (Pa)	$\tau_{c,avg}$ (Pa)
Low yield area, near-surface claypan layer in Figure 4.6(A)	Surface	J-1	09/20/18	5.00	5.18
		J-3	02/07/19	5.68	
		J-5	07/12/19	4.87	
	25 cm Below Surface	J-2	09/20/18	15.06	15.19
		J-4	07/02/19	15.31	
High yield area, no near-surface claypan layer in Figure 4.6(B)	Surface	J-7	09/20/18	3.75	4.23
		J-8	07/11/19	4.85	
		J-9	07/11/19	4.08	
	25 cm Below Surface	J-6	07/11/19	18.23	17.18
		J-10	07/11/19	16.12	

Chapter 5 - Discussion

Variation in near-surface soil erosion was investigated to determine if undermining of surface soil was attributed to an underlying claypan layer and if the depth to the claypan layer influenced the rate of surface soil erosion. One geophysical method was used to highlight areas of near-surface claypan layers (i.e., EC_a Mapping). A related geophysical method was used to determine the differences in soil stratigraphy between an area with a near-surface claypan layer and an area with no underlying claypan layer (i.e., ERT). While EC_a identified bulk areas of interest, ERT was able to identify areas where a near-surface claypan layer existed and areas where it did not exist. This was used to more accurately guide sample collection. Soil samples were collected utilizing ERT surveys to determine the soil classification, undrained shear strength, and hydraulic conductivity of an area with a near-surface claypan layer and an area with no underlying claypan layer. Two different erosion tests were performed (i.e., EFA test and JET) to determine the critical shear stress of the surface soil and claypan layer. The EFA was used because it can test at much higher hydraulic shear stresses and because undisturbed samples were collected, which allowed for testing the claypan layer at greater depths below the surface. Recall Sample 4, collected from site one in a high EC_a, low yield area, did not erode until 6 m s^{-1}. The advantage of the JET was its ability to perform tests in situ with minimum soil disturbance. The JET apparatus was used to test at the surface and 25 cm below the surface to show how rapidly the critical shear stress increases with depth in this claypan region. Note it was not possible to dig a hole deep enough to reach a comparable depth from which EFA samples were collected. Therefore, we used two different erosion tests to fully explore the erodible layers at these unique sites.

Site one. The low electrical resistivity measurements (10 Ohm-m or less) near the surface in Survey 1A (Figure 4.2) directly correlated to the area of highest EC_a measurements and lowest corn yield measurements in Figure 4.1. The electrical resistivity measurements in Survey 1A indicated a claypan layer at the surface but soil classification of Sample 1 indicated a lean clay layer overlying a fat clay layer (Table 4.1). The hydraulic conductivity of Sample 3-1 (i.e., the lean clay layer) was 2.2E-5 cm s^{-1} and was two orders of magnitude higher than Sample 3-2 (i.e., the fat clay layer) with a hydraulic conductivity of 9.1E-7 cm s^{-1} (Table 4.1). The undrained shear strength of the underlying fat clay layer (Sample 2-2) was 103 kPa and about two times higher than the overlying lean clay layer (Sample 2-1), which was 47 kPa. This supports the hypothesis

that although the near-surface soils are clay, there are in fact two distinct near-surface clay layers that may be enhancing the erosion of the overlying surface soil layer (i.e., lean clay) by the process of undermining.

As previously noted, Sample 7 collected in the low EC_a area from site one contained a lean clay layer overlying a fat clay layer and shared a similar trend in undrained shear strength (Sample 8) and hydraulic conductivity (Sample 9) as Samples 2 and 3 collected in the high EC_a area (Table 4.1). The undrained shear strength of the underlying fat clay layer (Sample 8-2) was about two times higher (64 kPa) than the overlying lean clay soil (Sample 8-1) which was 33 kPa. The hydraulic conductivity of the lean clay layer (Sample 9) collected where no underlying claypan layer existed was 5.1E-3 cm s^{-1} which was two orders of magnitude higher than the hydraulic conductivity of the lean clay layer (Sample 3-1) where a near-surface claypan existed (Table 4.1). Even though similar undrained shear strength and hydraulic conductivity trends are shared between the high and low ECa area, the undrained shear strength was relatively lower in Samples 2-1 and 8.1. The observed ERT data and corn yield map also indicated the area where there was no existing near-surface claypan layer supporting the hypothesis that the claypan is not uniform across the site as previously believed.

The critical shear stress of soil describes the erosion potential. The higher the critical shear stress the more resistant the soil is to erosion and the lower the critical shear stress the more erodible the soil. With that, the fat clay layer (Sample 4) in the high EC_a area at site one had a critical shear stress of 118.26 Pa and the lean clay layer in the transition (Sample 6) and low EC_a (Sample 10-1) area had a critical shear stress of 19.43 Pa and 18.73, respectively (Table 4.1). Having a higher hydraulic conductivity and more erodible soil layer overlying a lower hydraulic conductivity and more erosion-resistant claypan layer suggests that water flows through the surface soil to the impermeable claypan layer. When the water reaches the impermeable claypan layer, it likely flows laterally creating a perched water table. According to Kitchen et al. (2005), the presence of a perched water may exacerbate erosion of the topsoil. The increased erosion of a surface soil overlying a claypan layer inherently decreases surface soil thickness eventually exposing the claypan layer at the surface resulting in much greater runoff potential. This was evident where the JET was performed 25 cm below the surface in an area where the near-surface claypan layer existed. The critical shear stress determined in the high EC_a area (i.e., Surveys 1(A-B)) using the JET showed a lower average critical shear stress of 8.0 Pa for tests performed at the

surface (i.e., J-4,J-6, and J-7) and relatively higher average critical shear stress of 16.0 at the claypan layer about 25 cm below the surface (i.e., J-1, J-2, and J-5) (Table 4.2). Interestingly, the average critical shear stress in a low EC_a area (i.e., Surveys 1(C-D)) was 6.0 Pa at the surface (i.e., J-9, J-13, and J-14) and 7.0 Pa at a depth 25 cm below the surface (i.e., J-10, J-11, and J-12) (Table 4.2). Overall the range of critical shear stress values performed in a low EC_a area were lower where there was no near-surface claypan layer, whereas the critical shear stress was higher at the claypan layer. Again, the critical shear stress determined from the JET highlighted a highly erodible thin lean clay layer overlying a more erosion-resistant fat clay layer (i.e., claypan layer) in the high EC_a area. Conversely, the critical shear stress values determined at the surface and 25 cm below the surface in the low EC_a area highlighted a more uniformly erodible soil. Again, this observation supports the relatively lower undrained shear strength soil in areas of the ERT data where no claypan layer existed, highlighting the variability of the claypan layer across the site.

Site two. Like the ERT surveys and EC_a map from site one, the low electrical resistivity measurements (Figure 4.6(A)) directly correlated to low corn yield in a high EC_a area (Figure 4.5). The low electrical resistivity measurements (10 Ohm-m or less) highlighted a thick claypan layer at the surface in Survey 2A. Interestingly, unlike site one, two layers (CL overlying CH) were only observed in Sample 5, which was collected in the transition area from Survey 2B. However, one layer was observed in Samples 1 and 7 in the high and low ECa area, respectively. Samples 1 and 7 were classified as a lean clay soil. This finding was very unexpected because the claypan layer, a low resistivity layer (10 Ohm-m or less), at site one was classified as a fat clay soil, whereas the claypan layer at site two was classified as a lean clay soil. The hydraulic conductivity of the lean clay soil (Sample 9) in the low EC_a area (Survey 2B) was one order of magnitude higher (2.2E-5 cm s^{-1}) than the lean clay soil (Sample 3) in the high EC_a area (1.7E-6 cm s^{-1}). The lean clay soil in Survey 2B had a higher hydraulic conductivity than the lean clay soil in Survey 2A indicating that water would flow more easily through the subsurface in Survey 2B than Survey 2A, which is more likely to flow laterally across the surface as runoff due to the low hydraulic conductivity of the soil.

Previous research has correlated the soil undrained shear strength to susceptibility to erosion where higher undrained shear strength soils are more resistant to erosion and lower undrained shear strength soils are more erodible, although recent research has found no correlation between soil undrained shear strength and erosion susceptibility (Karim and Kulesza, in review).

The undrained shear strength results presented in this research were used to validate the presence of soil layers determined from soil classification. In Table 4.3, the undrained shear strength of Sample 2-2, collected in the high EC_a area from Survey 2A, was about two times higher (60 kPa) than Sample 2-1 which had a undrained shear strength of 28 kPa. This suggested there were two layers present in this sample even though one layer was observed from soil classification. Sample 8, collected in the low EC_a area from Survey 2B, had an undrained shear strength of 42 kPa and 47 kPa, respectively. This confirmed the presence of one layer in Sample 8 collected in this low EC_a area.

The same procedure for interpretation of critical shear stress values determined from the EFA test and JET followed site one. The critical shear stress values between a high and low EC_a area from the EFA test followed a similar trend as site one. Sample 4, collected in the high EC_a area, had a critical shear stress of 20.6 Pa, whereas Sample 10, collected in the low EC_a area, had a critical shear stress of 5.34 Pa. The critical shear stress of Sample 4 was about four times higher than Sample 10. The critical shear stress values determined from the EFA test indicated the lean clay soil in Survey 2A was more erosion-resistant than the lean clay soil in the low EC_a area from Survey 2B.

Like site one, the JET performed at the surface in Surveys 2A and 2B (i.e., J-1, J-3, J-5, J-7, J-8, and J-9) were relatively lower than the JET performed 25 cm below the surface (i.e., J-2, J-4, J-6, and J-10). The average critical shear stress performed at the surface in the high EC_a area (i.e., J-1, J-3, and J-5) was 5.0 Pa, whereas in the low EC_a area (i.e., J-7, J-8, and J-9) the average critical shear stress was 4.0 Pa. The average critical shear stress determined from the JET performed 25 cm below the surface in Survey 2B (i.e., J-6 and J-10) was 1.0 Pa, whereas the average critical shear stress at the claypan layer in Survey 2A (i.e., J-2 and J-10) was 15.0 Pa. Interestingly, the average critical shear stress value 25 cm below the surface in the high and low EC_a area were similar (within 1 Pa). This suggested that the JET were not performed in an area where there was no near-surface claypan layer. Lower critical shear stress values were expected where there was no claypan layer at the surface and higher critical shear stress values were expected at the claypan layer. One additional JET was performed 25 cm below the surface in a low EC_a area and confirmed the relatively higher critical shear value in Survey 2B than in Survey 2A. The relatively lower average critical shear stress observed at the surface in the high and low EC_a area highlighted the presence of a thin more erodible lean clay layer overlying a less erodible

claypan layer not shown in Surveys 2A and 2B. Interestingly, the critical shear stress determined from the JET performed at the surface in the low EC_a area (Survey 2B) had lower critical shear stress values than all other JET performed at the surface between both sites. Like site one, the JET results in Table 4.4 supports the hypothesis that surface soil is being undermined due to an underlying impermeable claypan layer. The JET performed in the low EC_a area (Survey 2B) did not extend far enough to capture an area where there was no near-surface claypan layer. This was evident by the similar average critical shear stress value observed 25 cm below the surface between the high and low EC_a area (Table 4.4).

Chapter 6 - Conclusions

The objective of this research was to delineate the variability of soil properties, including soil erodibility, in claypan soils. Understanding how soil properties change in the subsurface is critical to understanding the processes exacerbating soil loss in claypan regions. The data from this research show that the claypan layer is spatially variable within and between both sites. The extent of spatial variability of the claypan layer is likely contributing to different rates of erosion of the overlying surficial soil. The claypan layer is higher in undrained shear strength, lower in hydraulic conductivity, and more erosion-resistant. The measured range in critical shear stress between two distinct soil layers indicated that the rate and extent of soil erosion from within both sites was highly variable and based upon soil stratigraphy.

Laboratory erosion test results (i.e., EFA) found the claypan layer was characterized as low erodibility; conversely the surficial soil was classified as moderate erodibility. Results indicated the low erodible soil had higher undrained shear strength but lower hydraulic conductivity. Conversely, the moderate erodible soil indicated a lower undrained shear strength and soil with higher hydraulic conductivity. Therefore, the presence of a higher undrained shear strength/lower hydraulic conductivity soil underlying a lower undrained shear strength/higher hydraulic conductivity soil is likely increasing the rate of surficial soil erosion by undermining at the interface. In situ erosion test results (i.e., JET) showed how rapidly erosion potential changed from the surface of the soil to a depth 25 cm below the surface. Results from both erosion tests (i.e., EFA and JET) showed a similar trend in that the surficial soil was more erodible (i.e., had a lower critical shear stress) than the claypan layer, which had a higher critical shear stress value. Limitations of this research includes the number of EFA tests performed on samples collected in the high and low EC_a areas, the number of JET performed at the surface and 25 below the surface at both sites, and the number of claypan sites investigated. The data from this research will aid in the improvement of soil management practices and existing erosion models at field and watershed scales. This research shows how variable subsurface composition is within a site and region.

6.1 Recommendations

Recommendations learned from this research includes measuring erosion at the surface and at a predetermined depth (e.g., 25 cm) below the surface across the sites to integrate erosion data into erosion models. The erosion results, from this research, between two sites with the same land management procedures highlighted how variable erosion was within and between the sites. The

collection of more erosion data across sites would likely improve erosion model accuracy of predicting erosion at field and watershed scales. I would also recommend the use of geophysics to identify areas of interest within a site allowing for a more strategic testing procedure. The use of geophysical methods to identify near-surface soil changes can also improve the accuracy of predicted soil erosion in soil models. Monitoring the flow of water through the subsurface may aid in understanding how different soil layers affect each other and may improve the quantification of soil loss at the surface. I would recommend the use of cover crops in areas within a site where a claypan layer exists near-surface. Cover crops planted in near-surface claypan areas may aid in the breaking up of this impervious clay layer and provides greater access to necessary nutrients for crop growth.

6.2 Future work

In this study, the number of erosion tests should be increased to increase the amount of erosion data between a high and low EC_a area in a claypan region. The self-potential test (a passive geophysical measurement) should be performed to validate the predicted flow of water at the claypan layer and surface soil interface. Two self-potential tests were conducted in this research; however the results were affected by power transmission lines over the claypan area resulting in noise in the dataset. Other sites with claypan soils but without external sources of noise should be used to conduct the self-potential tests. The erosion results from this research should be used to quantify soil loss in erosion models.

References

Abu-Hassanein, Z. S., Benson, C. H., & Blotz, L. R. (1996). Electrical resistivity of compacted clays. *Journal of Geotechnical Engineering, 122(5), 397-406*.

AGI (Advanced Geosciences, Inc.). (2008). Instruction Manual for EarthImager 2D Version 2.4.0 Resistivity and IP Inversion Software, Advanced Geosciences, Inc., Austin TX.

Al-Madhhachi, A. T., Hanson, G. J., Fox, G. A., Tyagi, A. K., and Bulut, R. (2013). Measuring soil erodibility using a laboratory "mini" JET. *Trans. ASABE, 56(3), 901-910*.

Al-Madhhachi, A. T., Hanson, G. J., Fox, G. A., Tyagi, A. K., and Bulut, R. (2011). Measuring erodibility of cohesive soils using laboratory jet erosion tests. *World Environmental and Water Resources Congress ASCE, 2350-2359*.

Arjwech, R., Everett, M.E., Briaud, J.-L., Hurlebaus, S., Medina-Cetina, Z., Tucker, S., and Yousefpour, N. (2013). Electrical resistivity imaging of unknown bridge foundations, Near Surf. Geophys., 11(6), 591-598. http://doi.org/10.3997/1873-0604.2013023

Arneson, L. A., Zevenbergen, L. W., Lagasse, P. F., & Clopper, P. E. (2012). *Evaluating scour at bridges* (No. FHWA-HIF-12-003).

ASTM. (2017). C117-17: Standard Test Method for Materials Finer than 75-μm (No.200) Sieve in Mineral Aggregates by Washing. West Conshohochen, PA: ASTM Int.

ASTM. (2015). C136/C136M-14: Standard Test Method for Sieve Analysis of Fine and Coarse Aggregates. West Conshohochen, PA: ASTM Int.

ASTM. (2010). D2216-10: Standard Test Method for Laboratory Determination of Water (Moisture) Content of Soil and Rock by Mass. West Conshohochen, PA: ASTM Int.

ASTM. (2015). D2850-15: Standard Test Method for Unconsolidated-Undrained Triaxial Compression Test on Cohesive Soils. West Conshohochen, PA: ASTM Int.

ASTM. (2017). D4318-17e1: Standard Test Methods for Liquid Limit, Plastic Limit, and Plasticity of Soils. West Conshohochen, PA: ASTM Int.

ASTM. (2016). D5084-16a: Standard Test Methods for Measurement of Hydraulic Conductivity of Saturated Porous Material Using a Flexible Wall Permeameter. West Conshohochen, PA: ASTM Int.

ASTM. (2017). D7928-17: Standard Test Method for Particle-Size Distribution (Gradation) of Fine-Grained Soils Using the Sedimentation (Hydrometer) Analysis. West Conshohochen, PA: ASTM Int.

Bernhardt, M., Briaud, J-L., Kim, D., Leclair, M., Storesund, R., Lim, S.-G., and Rogers, J. D., (2011). Mississippi river levee failures: June 2008 flood. *Int. J. Geoengineering Case Histories, 2(3), 127-162*.

Bernstone, C., Dahlin, T., Ohlsson, T., and Hogland, H. (2000). DC Resistivity mapping of internal landfill structures: Two pre-excavation surveys. *Environ. Geol., 39(3-4), 360-371*. https://doi.org/10.1007/s002540050015

Binley, A., & Kemna, A. (2005). DC resistivity and induced polarization methods. In *Hydrogeophysics* (pp. 129-156). Springer Netherlands.

Blanco-Canqui, H., Gantzer, C. J., Anderson, S. H., Alberts, E. E., and Ghidey, F. (2002). Saturated hydraulic conductivity and its impact on simulated runoff for claypan soils. *SSSJ, 66(5), 1596-1602. https://doi.org/10.2136/sssaj2002.1596*

Briaud, J. L., Ting, F., Chen, H. C., Cao, Y., Han, S. W., and Kwak, K. W. (2001). Erosion Function Apparatus for Scour Rate Predictions. *Journal of Geotechnical and Geoenvironmental Engineering, 127(2), 105–113.* https://doi.org/10.1061/(ASCE)1090-0241(2001)127:2(105)

Buckley, M., Kluitenberg, G., Sweeney, D., Kelley, K., and Stone, L. (2008). Effect of tillage on the hydrology of a claypan soil in Kansas. *Soil Sci. Soc. Am. J., 74, 2109-2119*.

Butler, D. K. (2005). Near-Surface Geophysics. *Society of Exploration Geophysicists*. Tulsa, OK.

Corwin, D.L., Lesch, S.M., Shouse, P.J., Soppe, R., and Ayars, J.E. (2003b). Identifying soil properties that influence cotton yield using soil sampling directed by apparent soil electrical conductivity. *Agron. J., 95 (2), 352–364*.

Daly, E. R., Fox, G. A., Al-Madhhachi, A. S. T., and Miller, R. B. (2013). A scour depth approach for deriving erodibility parameters from jet erosion tests. *Trans. ASABE, 56(6), 1343-1351*.

Doolittle, J. A., Sudduth, K. A., Kitchen, N. R., and Indorante, S. J. (1994). Estimating depths to claypans using electromagnetic induction methods. *Journal of Soil Water Conservation, 49, 572-575.*

Everett, M.E. (2013). Near-surface applied geophysics. New York, NY: Cambridge University Press. https://doi.org/10.1017/CBO9781139088435

Fanning, C.D. and Gray, F. (1959). Characterization and genetic study of a Dennis and a Parsons soil. *Soil Sci. Soc. Am. J., 23, 321–324*.

Friedman, S. P. (2005). Soil properties influencing apparent electrical conductivity: A review. *Comput. Electron. Agric., 46(1), 45-70*. http://dx.doi.org/10.1016/j.compag.2004.11.001

Frischknecht, F. C. and Keller, G. V. (1966). *Electrical methods in geophysical prospecting.* Pergamon Press.

Fukue, M., Minato, T., Horibe, H., & Taya, N. (1999). The micro-structures of clay given by resistivity measurements. *Engineering Geology, 54(1), 43-53*.

Giao, P. H., Chung, S. G., Kim, D. Y., & Tanaka, H. (2003). Electric imaging and laboratory resistivity testing for geotechnical investigation of Pusan clay deposits. *Journal of Applied Geophysics, 52(4), 157-175*.

Grabowski, R. C., Droppo, I. G., & Wharton, G. (2011). Erodibility of cohesive sediment: the importance of sediment properties. *Earth-Science Reviews, 105(3), 101-120*.

Groves, P., Cascante, G., Dundas, D., and Chatterji, P. K. (2011). Use of geophysical methods for soil profile evaluation. *Canadian Geotech. J., 48(9), 1364-1377*. https://doi.org/10.1139/t11-044

Hallof, P. (1957). On the interpretation of resistivity and induced polarization measurements. Ph.D. thesis, MIT, Cambridge, U.K.

Hanson, G. J. (1996). Investigating soil strength and stress-strian indices to characterize erodibility. *Trans. ASAE, 39(3), 883-890*.

Hanson, G. J. (1991). Development of a jet index to characterize erosion resistance of soils in earthen spillways. *Trans. ASAE, 34(5), 2015-2020*.

Hanson, G. J. (1990a). Surface erodibility of earthen channels at high stresses: I. Open channels testing. *Trans. ASAE, 33(1), 127-131*.

Hanson, G. J. (1990b). Surface erodibility of earthen channels at high stresses: II. Developing an *in situ* testing device. *Trans. ASAE, 33(1), 132-137*.

Hanson, G. J. and Cook, K. R. (2004). Apparatus, test procedures, and analytical methods to measure soil erodibility *in situ*. *Appl. Eng. Agricul., 20(4), 455-462*.

Hanson, G. J. and Cook K. R. (1997). Development of excess shear stress parameters for circular jet testing. *ASAE Paper No. 972227. St. Joseph, Mich.: ASAE.*

Hanson, G. J., Robinson, K. M., and Cook, K. R. (2002). Scour below an overfall: Part II. Prediction. *Trans. ASAE, 45(4), 957-964*.

Hartley, P.E., Presley, D. R., Ransom, M. D., Hettiarachchi, G. M., and West, L. T. (2014). Vertisols and Vertic Properties of Soils of the Cherokee Prairies of Kansas. *Soil Sci. Soc. Am. J., 78, 556-566*.

Hillel, D. (2004). *Introduction to environmental soil physicals*. Elsevier Science. Academic Press. Amsterdam.

Hiltunen, D. and Roth, M. (2003). Investigation of bridge foundation sites in Karst Terrane via multi-electrode electrical resistivity. Proc. 3rd Int. Conf. on Applied Geophysics. Washington, DC: FHWA.

Jamison, V. C., Smith, D. D., and Thornton, J. F., (1968). Soil and water research on a claypan soil. USDA Tech. Bull. 1379. Washington, DC: U.S. Government Printing Office.

Jaynes, D.B. (1996). Improved soil mapping using electromagnetic induction surveys. p. 169–179. In P.C. Robert et al. (ed.) *Precision agriculture.* Proc. Int. Conf., 3rd, Minneapolis, MN. 23–26 June 1996. ASA, CSSA, and SSSA, Madison, WI.

Jaynes, D.B., Colvin, T. S., and Ambuel, J. (1995). Yield mapping by electromagnetic induction. p. 383–394. In P.C. Robert et al. (ed.) *Site-specific management for agricultural systems.* Proc. Int. Conf., 2nd, Minneapolis, MN. 27–30 Mar. 1994. ASA, CSSA, and SSSA, Madison, WI.

Kamphius, W. J. and Hall, K. R. (1983). Cohesive material erosion by unidirectional current. *J. of Hydraulic Engineering, ASCE 109(1), 1076-1081*.

Kansas Water Office. (2016). John Redmond dredging initiative. Retrieved from http://www.kwo.org/projects/JohnRedmondDredging.html

Karamigolbaghi, M., Ghaneeizad, S. M., Atkinson, J. F., Bennet, S. J., and Wells, R. R. (2017). Critical assessment of jet erosion test methodologies for cohesive soil and sediment. *Geomorphology*. doi: 10.1016/j.geomorph.2017.08.005.

Karim, M.Z. and Tucker-Kulesza, S. (2018). Predicting soil erodibility using electrical resistivity tomography. *J. Geotech. Geoenviron. Eng. 144(4): 04018012.* https://doi.org/10.1061/(ASCE)GT.1943-5606.0001857

Kibria, G., and Hossain, M. S. (2012). Investigation of geotechnical parameters affecting electrical resistivity of compacted clays. *Journal of Geotechnical and Geoenvironmental Engineering, 138(12), 1520-1529*.

Kitchen, N. R., Drummond, S. T., Lund, E. D., Sudduth, K. A., and Buchleiter, G. W. (2003). Soil electrical conductivity and topography related to yield for three contrasting soil-crop systems. *Agron. J., 95(3),* 483-495.

Kitchen, N.R., Sudduth, K.A., and Drummond, S.T. (1996). Mapping of sand deposition from 1993 Midwest floods with electromagnetic induction measurements. *J. Soil Water Conserv., 51 (4), 336–340*.

Kitchen, N. R., Sudduth, K. A., Myers, D. B., Drummond, S. T., and Hong, S. Y. (2005). Delineating productivity zones on claypan soil fields using apparent soil electrical conductivity. *Comput. Electron. Agric., 46(1), 285-308*. http://dx.doi.org/10.1016/j.compag.2004.11.012

Knapen, A., Poesen, J., Govers, G., Gyssels, G., & Nachtergaele, J. (2007). Resistance of soils to concentrated flow erosion: A review. *Earth-Science Reviews, 80(1), 75-109*.

Kwader, T. (1985). Estimating aquifer permeability from formation resistivity factors. *Ground Water, 23(6), 762-766*.

Loke, M. H. (1999). *Electrical Imaging Surveys for Environmental and Engineering Studies*.

Lund E.D., Colin D. and Christy P.E. (1978). Using electrical conductivity to provide answers for precision farming. *1st International Conference Geospatial Information in Agriculture and Forestry*.

Mitchell, J. and Soga, K. (2005). *Fundamentals of soil behavior*, Wiley, Hoboken, NJ, USA.

Moody, L.F. (1944). Friction factors for pipe flow. *Trans. ASABE, 66(8), 671-684*.

Partheniades, E. (1965). Erosion and deposition of cohesive soils. *J. Hydraulics Div. ASCE, 91(1), 105-139*.

Rhoades, J. D., Manteghi, N. A., Shouse, P. J., and Alves, W. J. (1989). Soil electrical conductivity and soil salinity: New formulations and calibrations. *SSSAJ, 53(2), 433-439.* https://doi.org/10.2136/sssaj1989.03615995005300020020x

Sanford, L. P. (2008). Modeling a dynamically varying mixed sediment bed with erosion, deposition, bioturbation, consolidation, and armoring. *Computers & Geosciences, 34(10), 1263-1283*.

Schaetzl, R.J. and Thompson, M. (2015). Soil genesis and profile differentiation. p. 321–443. In *Soils: Genesis and Geomorphology*. 2nd ed. Cambridge University Press. Cambridge, England.

Schwab, G. O., Fangmeier, D. D., Elliot, W. J., and Frevert, R. K. (1993). *Soil and water conservation engineering.* 4th Edition. John Wiley and Sons, Inc. New York, 68-91.

Smerdon, E. T. and Beasley, R. P. (1959). The tractive force theory applied to stability of open channels in cohesive soils. Research Bulletin 715. University of Missouri. Ag. Exp. Station. Columbia, Mo.

Soil Science Terms Committee. (2008). Glossary of Soil Science Terms. *Soil Science Society of America*, Madison, WI.

Stein, O. P., Julien, P. Y., and Alonso, C. V. (1993). Mechanics of jet scour downstream of a headcut. *J. of the Hydraulic Research of IAHR, 31(6), 732-738.*

Tran, T. (2018). Instrumentation of erosion function apparatus and evaluation of a new erosion characterization methodology. Ph.D. Thesis, Department of Civil Engineering, Kansas State University.

Tran, T., Tucker-Kulesza, S., and Bernhardt, M. (2017). Determining Surface Roughness in Erosion Testing Using Digital Photogrammetry. *Geotechnical Testing Journal, 40(6), 917-927.*

Tucker, S. E., Briaud, J.-L., Hurlebaus, S., Everett Mark, E., and Arjwech, R. (2015). Electrical resistivity and induced polarization imaging for unknown bridge foundations. *J. Geotech. Geoenviron. Eng., 141*(5).

Van Klaveren, R. W., & McCool, D. K. (1998). Erodibility and critical shear of a previously frozen soil. *Trans. ASAE, 41(5), 1315*.

Wahl, T. L. (2016). The submerged jet erosion test: past-present-future. *USSD Int. Symp. Mech. Intern. Eros. Dams Levees*, Salt Lake City, UT, USA.

Watson, D. A. and Laflen, J. M. (1986). Soil strength, slope and rainfall intensity effects on interrill erosion. *Trans. ASAE, 29, 98-102*.

Winterwerp, J. C., & Van Kesteren, W. G. (2004). Introduction to the physics of cohesive sediment dynamics in the marine environment. *Elsevier Science, 56(1), 576*.

Appendix A - EFA Data

Table 6.1. Site one EFA results.

Sample I.D.	Erosion Test Results							Critical Shear Stress (Pa)
4	Water Velocity (m/s)	1	2	3	4	5	6	118.26
	Erosion Rate (mm/hr)	0.1	0.1	0.1	0.1	0.1	1.8	
	Shear Stress (Pa)	4.62	17.98	40.45	77.90	112.36	220.22	
6	Water Velocity (m/s)	1	2	3	4	5	6	19..43
	Erosion Rate (mm/hr)	0.1	0.1	2.4	7.8	-	-	
	Shear Stress (Pa)	4.49	17.98	52.81	91.88	-	-	
10-1	Water Velocity (m/s)	1	2	3	4	5	6	18.73
	Erosion Rate (mm/hr)	0.1	0.1	10.8	30	-	-	
	Shear Stress (Pa)	5.12	18.48	46.07	97.88	-	-	
10-2	Water Velocity (m/s)	1	2	3	4	5	6	74.79
	Erosion Rate (mm/hr)	0.1	0.1	0.1	0.1	15	16.8	
	Shear Stress (Pa)	4.24	17.48	49.44	73.91	152.93	220.22	

Table 6.2. Site two EFA results.

Sample I.D.	Erosion Test Results							Critical Shear Stress (Pa)
4	Water Velocity (m/s)	1	2	3	4	5	6	20.60
	Erosion Rate (mm/hr)	0.1	0.1	7.2	7.2	11.4	21.8	
	Shear Stress (Pa)	4.87	19.97	65.17	107.86	184.14	301.12	
6	Water Velocity (m/s)	1	2	3	4	5	6	5.52
	Erosion Rate (mm/hr)	0.1	1.8	3.6	7.2	112	288	
	Shear Stress (Pa)	4.49	22.97	58.43	81.90	159.17	247.19	
10	Water Velocity (m/s)	1	2	3	4	5	6	5.34
	Erosion Rate (mm/hr)	0.1	3	4.2	6	13.2	18.7	
	Shear Stress (Pa)	4.74	22.47	46.07	83.89	137.33	188.76	

Appendix B - "Mini" JET Data

Table 6.3. Near-surface claypan area erosion data at site one.

Time	Scour Measurements (mm)						
	Surface			25 cm Below Surface			
(min)	J-4	J-6	J-7	J-1	J-2	J-3	J-5
0	0	0	0	0	0	0	0
1	21	29	17	3	3	0	7
2	23	34	19	3	5	1	7
3	24	35	19	5	5	1	8
4	26	35	19	5	5	1	8
5	27	37	20	5	6	1	8
7	31	39	20	5	6	1	8
9	32	39	20	5	6	1	10
11	34	39	20	5	6	3	10
13	35	39	22	5	6	3	10
15	37	39	22	5	6	3	10
18	39	40	22	5	6	3	10
21	39	40	23	5	6	3	11
24	40	40	23	5	8	3	11
27	42	40	23	5	8	5	11
30	43	40	23	6	8	5	11
34	43	42	23	6	8	5	13
38	43	42	23	6	10	6	13
42	43	42	23	6	10	6	13
46	43	42	25	6	10	6	15
50	45	42	25	6	10	6	15
55	45	43	25	6	11	6	15
60	46	43	25	6	11	6	15
65	46	45	27	6	11	6	16
70	46	45	27	6	13	8	16
80	46	45	28	6	13	8	16
90	48	45	28	8	13	8	18
100	50	45	28	8	13	8	18
110	50	46	30	8	16	8	19
120	50	46	30	8	18	8	19

Table 6.4. No near-surface claypan area erosion data at site one.

Time	Scour Measurements (mm)						
	Surface			25 cm Below Surface			
(min)	J-9	J-13	J-14	J-8	J-10	J-11	J-12
0	0	0	0	0	0	0	0
1	28	21	27	3	13	3	16
2	32	26	29	3	18	3	16
3	33	27	30	10	18	3	18
4	33	29	32	10	21	3	20
5	35	30	34	11	22	3	21
7	35	32	35	13	26	5	26
9	36	32	35	14	38	5	27
11	36	34	37	18	40	10	29
13	36	37	37	19	43	10	32
15	36	38	38	21	43	11	32
18	36	40	38	21	45	11	34
21	38	41	38	22	45	13	34
24	38	43	40	22	45	14	34
27	38	45	40	24	46	18	34
30	40	46	40	24	46	21	35
34	40	46	41	26	46	22	35
38	40	48	41	26	48	24	35
42	40	48	41	27	48	25	35
46	41	48	41	27	51	25	35
50	41	49	41	27	52	25	35
55	41	49	41	27	52	25	35
60	41	49	41	29	57	25	35
65	41	49	43	29	57	25	35
70	43	51	43	29	59	25	35
80	43	51	43	30	59	27	35
90	44	51	43	30	62	27	37
100	44	53	46	30	62	29	37
110	44	53	46	32	64	30	37
120	46	53	46	32	65	30	37

Table 6.5. Summary of JET data for site one.

Area of Interest	Location	Sample I.D.	τ_c (Pa)	$\tau_{c,avg}$ (Pa)	ε (mm s^{-1})	τ_o (Pa)	$\tau_{o,avg}$ (Pa)
Low yield area, near-surface claypan layer in Figure 4.2(A-B)	Surface	J-4	6.29	7.71	0.00694	94.47	94.47
		J-6	6.80		0.00639	94.47	
		J-7	10.03		0.00417	94.47	
	25 cm Below Surface	J-1	16.75	15.54	0.00111	94.47	94.22
		J-2	16.48		0.0025	94.47	
		J-3	25.32		0.00111	93.46	
		J-5	13.40		0.00264	94.46	
High yield area, no near-surface claypan layer in Figure 4.2(C-D)	Surface	J-9	7.33	6.17	0.00639	94.47	94.47
		J-13	5.05		0.00736	94.47	
		J-14	6.13		0.00639	94.47	
	25 cm Below Surface	J-8	12.00	7.10	0.00444	93.46	93.97
		J-10	4.97		0.00903	93.46	
		J-11	7.83		0.00417	94.47	
		J-12	8.51		0.00514	94.47	

Table 6.6. Near-surface claypan area erosion data at site two.

Time	Scour Measurements (mm)				
	Surface			25 cm Below Surface	
(min)	J-1	J-3	J-5	J-2	J-4
0	0	0	0	0	0
1	21	19	16	5	1
2	21	26	20	5	3
3	24	27	27	5	3
4	24	27	28	7	3
5	29	29	28	7	3
7	31	30	30	7	5
9	31	30	35	7	5
11	33	30	38	8	5
13	34	32	39	8	6
15	34	32	39	8	6
18	34	32	41	10	6
21	35	34	42	10	6
24	35	35	42	10	6
27	39	37	42	10	6
30	40	37	44	10	8
34	42	37	44	10	8
38	42	38	44	10	8
42	45	40	46	12	8
46	45	40	46	12	8
50	46	41	46	12	8
55	46	41	46	12	8
60	50	41	47	12	8
65	50	41	47	12	9
70	51	43	49	12	9
80	54	43	49	12	9
90	56	43	50	12	11
100	58	43	50	12	13
110	58	43	50	12	13
120	58	45	52	12	13

Table 6.7. No near-surface claypan area erosion data at site two.

Time	Scour Measurements (mm)				
	Surface			25 cm Below Surface	
(min)	J-7	J-8	J-9	J-6	J-10
0	0	0	0	0	0
1	18	16	19	2	2
2	22	30	40	2	2
3	22	35	41	2	2
4	24	36	43	4	2
5	24	38	44	4	2
7	27	39	47	4	5
9	32	39	49	4	5
11	35	39	49	5	6
13	38	39	51	5	6
15	41	41	52	5	8
18	43	42	54	7	8
21	45	44	54	7	10
24	45	44	54	8	11
27	45	44	55	8	11
30	46	44	57	8	11
34	49	44	57	8	13
38	51	46	59	8	13
42	54	46	59	8	13
46	56	47	60	10	13
50	57	47	60	10	14
55	61	47	60	10	14
60	61	49	62	10	14
65	61	49	62	10	14
70	61	49	62	10	14
80	61	50	62	10	16
90	61	50	62	10	16
100	61	52	63	10	18
110	61	52	65	12	18
120	61	54	65	21	19

Table 6.8. Summary of JET data for site two.

Area of Interest	Location	Sample I.D.	τ_c (Pa)	$\tau_{c,avg}$ (Pa)	ε (mm s^{-1})	τ_o (Pa)	$\tau_{o,avg}$ (Pa)
Low yield area, near-surface claypan layer in Figure 4.6(A)	Surface	J-1	5.00	5.18	0.00806	89.39	86.34
		J-3	5.68		0.00625	85.33	
		J-5	4.87		0.00722	84.31	
	25 cm Below Surface	J-2	15.06	15.19	0.00333	93.46	92.95
		J-4	15.31		0.00181	92.44	
High yield area, no near-surface claypan layer in Figure 4.6(B)	Surface	J-7	3.75	4.23	0.01694	83.30	84.65
		J-8	4.85		0.0075	85.33	
		J-9	4.08		0.00903	85.33	
	25 cm Below Surface	J-6	18.23	15.62	0.00292	85.33	85.33
		J-10	13.00		0.00264	85.33	

Appendix C - Inverted ERT Sections

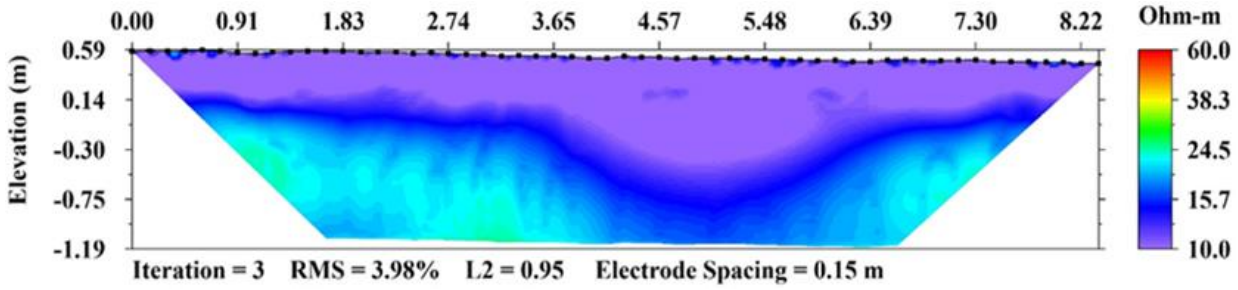

Figure 6.1.Inverted resistivity section between Surveys 1A and 1B.

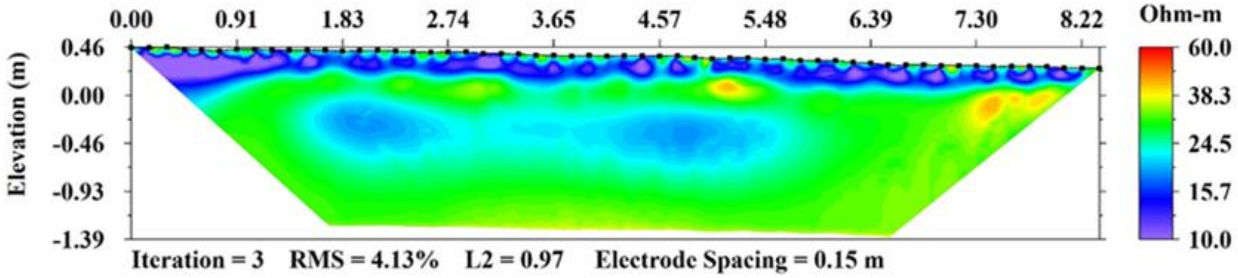

Figure 6.2. Inverted resistivity section between Surveys 1B and 1C.

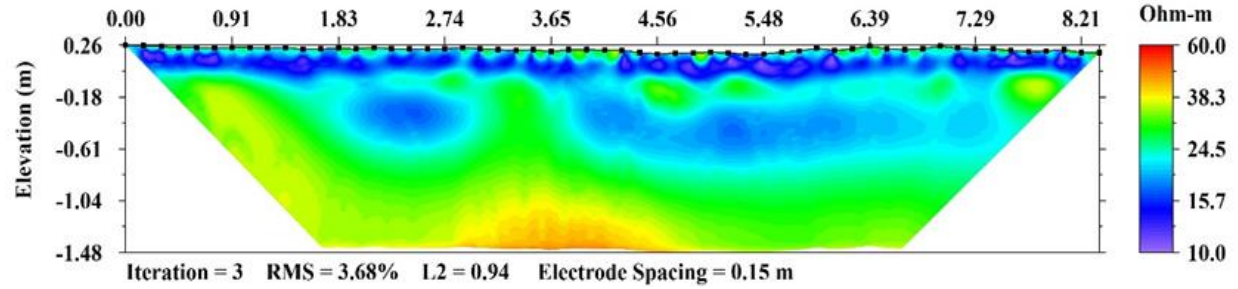

Figure 6.3. Inverted resistivity section between Surveys 1C and 1D.

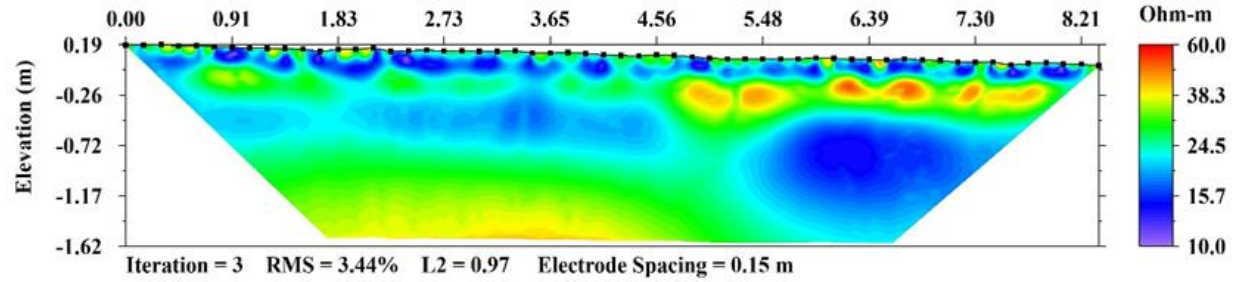

Figure 6.4. Inverted resistivity section overlapping Survey 1D at the midpoint.